

RUDIMENTARY SYNTHESSES OF SOLUTION PROCESSABLE
POLYANILINE AND GRAPHENE OXIDE MATERIALS
FOR ENERGY DEVICE APPLICATIONS

By

OMAR TALIB MELTON

A THESIS

Submitted in partial fulfillment of the requirements
for the degree of Master of Science in the
Applied Chemistry Graduate Program
of Department of Chemistry

DOVER, DELAWARE
August 2017

This thesis is approved by the following members of the Final Oral Review Committee:

Dr. Young-Gi Kim, Committee Chairperson, Department of Chemistry, Delaware State University

Dr. Andrew Goudy, Committee Member, Department of Chemistry, Delaware State University

Dr. Cherese Winstead-Casson, Committee Member, Department of Chemistry, Delaware State University

Dr. Mohammad Amir Khan, External Committee Member, Department of Physics & Engineering, Delaware State University

© Omar Talib Melton

All Rights Reserved

DEDICATION

بِسْمِ اللَّهِ الرَّحْمَنِ الرَّحِيمِ

I would like to dedicate this work

...to my mother, Phyllis Ann Lyons, for loving me

to my mother, Phyllis Ann Lyons, for providing for me

to my mother, Phyllis Ann Lyons, for encouraging me

and to my father, Carlos Melton Sr., for the same...

I would also like to dedicate this work to my brother, Christopher Lang Lyons, who passed on the 23rd of May 2016, of all the times I imagined the future you were never not there.

ACKNOWLEDGMENT

“He has not thanked God who has not thanked people.”

-Prophet Muhammad ﷺ

Any success I achieve belongs, in part, to those who supported me. First, I like to thank my mother, Phyllis Ann Lyons, for her constant love and unconditional support. I thank my wife, Siti Jayanti Rahmatina, for the many words of reassurance and cheer. I would like to thank Dr. Sakkar Eva, who encouraged me to apply to Delaware State University (DSU). My undergrad professors at Cheyney University, Dr. Warren Gooden, Dr. Donald Ford, Dr. Tony Dent, and Dr. Eva inspired me to try harder and they never stopped believing in me. Dr. Mazen Shahin and Latoya Stephens, from the Bridge to the Doctorate (BtD) program at DSU, and Dr. Stephen Cox and Venice Keene, from the Greater Philadelphia Region Louis Stokes Alliance for Minority Participation, supported me and advised me beyond what was necessary. I sincerely thank them all. Thanks are due to all my classmates at DSU and cohorts in the BtD program, but specifically Lewis Lott, Martin Chi, Deidre Carter, and Jasmine Smalls for giving me their support in my academic and research activities. Thanks to my lab mates Dan Yang and Wafaa Abousamra for their help and to Mr. Todd Campbell and Mr. Gregory Hopkins for some of the instrumentation. I thank all my professors in the Department of Chemistry at DSU for all their efforts in my education, guidance, and encouragement. Special thanks to Dr. Stacy L. Smith who made herself available for me to complete a portion of my research. I thank my committee members, Dr. Mohammad Amir Khan, Dr. Cherese Winstead-Casson, and Dr. Andrew Goudy. They have offered me their full support and advise for the completion of my research project. My final thanks goes to Dr. Young-Gi Kim. His intelligence guided me, his passion inspired me, and his patience encouraged me. I apologize to anyone whom I forgot to mention, but please know I fully appreciate anyone who takes time from their life to share it with mine.

Rudimentary Syntheses of Solution Processable Polyaniline and Graphene Oxide Materials for Energy Device Applications

Omar T. Melton

Faculty Advisor: Dr. Young-Gi Kim

ABSTRACT

Electrically conductive polymers (CPs) play a major role in organic electronics and are alternatives to traditional energy and electronic materials. The focus of this research is the rudimentary syntheses of polyaniline (PANI) as a processable and electrically conductive polymer, graphene oxide (GO) and reduced graphene oxide (rGO) materials for energy conversion or storage device. Novel and augmented syntheses are conducted intended for the improvement of processability, conductivity, and development of PANI and GO material film. We have observed that the bulky dopant, dioctylsulfosuccinate sodium salt (DSS), improved the solubility of PANI. The variation of solvent was attempted to increase the electrical conductivity, with *o*-xylene showing improved dispersion capability over toluene. Additionally, the synthesized PANIs exhibited differences in both film formation and conductivity. GO was produced from a variation of a modified Hummers' method. This new method incorporated the use of inexpensive commercial materials working toward the synthesis, purification, and development of GO. Bulky commercial grade graphite powder was used in place of the typical graphite flakes. Furthermore, cellulose filter paper was coopted in place of the standard metal sieve. Through effective grinding of graphite, the resultant synthesized material was good quality GO. Afterwards, thermal treatment applied under vacuum successfully reduced GO. The subsequent films fabricated from heat treated GO showed crystalline structure and improved conductivity over other GO materials.

TABLE OF CONTENTS

LIST OF TABLES	viii
LIST OF FIGURES	ix
LIST OF ABBREVIATIONS.....	xiii
CHAPTER 1. INTRODUCTION	1
1.1 Rationale.....	1
1.2 Electrically Conductive Polymers and Their Energy Applications.....	3
1.2.1 Polymer Photovoltaic Cells.....	8
1.2.1 Polymer Fuel Cells.....	10
1.2.2 Polymer Ion Battery	11
1.2.3 Polymer Supercapacitors.....	13
1.3 Thesis Objective	16
CHAPTER 2. LITERATURE REVIEW	17
2.1 Polyaniline.....	17
2.1.1 Synthesis of PANI.....	17
2.1.2 Doping of PANI.....	20
2.1.3 Characterization of PANI.....	22
2.2 Graphene Oxide.....	23
2.2.1 Synthesis of GO	23
2.2.2 Characterization of GO	24

2.3 PANI-Oxide Energy Devices	25
2.3.1 PANI Nanowires on GO for Energy Storage	25
CHAPTER 3. EXPERIMENTAL.....	29
3.1 Materials	29
3.2 Characterization Equipment	29
3.3 Synthesis of DSS Doped PANI	30
3.4 Secondary Doping of DSPA.....	31
3.5 Fabrication of DSPA Films	31
3.6 Synthesis of Graphene Oxide Materials	32
3.7 Fabrication of GO and rGO Films.....	33
CHAPTER 4. RESULTS AND DISCUSSION.....	35
4.1 DSPA Characterization.....	35
4.1.1 DSPA ¹ H NMR	35
4.1.2 DSPA Solution Optical Microscopy	37
4.1.3 DSPA Solution UV-Vis Spectra	38
4.1.4 DSPA _X Film UV-Vis Spectra	40
4.1.5 DSPA _X Film SEM.....	42
4.1.6 DSPA _X Film Surface Resistance.....	43
4.2 GO Materials Characterization.....	44
4.2.1 GO Materials FTIR	44

4.2.2	GO Materials Solution UV-Vis Spectra.....	47
4.2.3	GO Materials Optical Microscopy	50
4.2.4	GO Material Films SEM	52
4.2.5	GO Materials Surface Resistance.....	53
CHAPTER 5. CONCLUSION.....		54
5.1	Summary.....	54
REFERENCES		55

LIST OF TABLES

Table 1. Some conducting polymers, their structure, conductivity, and type/doping. ¹³	8
Table 2. Polymer energy devices type and source.	15
Table 3. Common PANI dopants.....	21
Table 4. Surface resistance of DSPA _x films.....	44
Table 5. Surface resistance of GO materials.....	53

LIST OF FIGURES

Figure 1. Electricity production by source. ³	1
Figure 2. CO ₂ emissions from energy consumption. ⁵	2
Figure 3. CO ₂ emissions by fuel type. ⁶	2
Figure 4. Homopolymer and copolymers.	3
Figure 5. Polymer chain representations. ⁸	3
Figure 6. Polymerization mechanisms.	4
Figure 7. Electrically conductive polymers.	5
Figure 8. Conductivity of materials.	5
Figure 9. π -bond electron delocalization.	6
Figure 10. Energy band gap of materials.	6
Figure 11. Charge transfer complexes formed form doping	7
Figure 12. New energy band gap as the result of doping.....	7
Figure 13. Solar cell schematic.	9
Figure 14. Chemical structure of the photoactive materials, stack structure of the tandem heterojunction device, and EQE spectra. ¹⁹	10
Figure 15. PEM fuel cell. ²²	11
Figure 16. Schematic of CPs in cell assemblies. ²⁷	12
Figure 17. Schematic view of battery cells. ²⁸	13
Figure 18. Schematic view of a SC. ²⁹	13
Figure 19. Charging mechanisms of SCs. ²⁹	14

Figure 20. Schematics of the fabrication process of thin 3D porous graphite foams and their integrated composites. ³³	15
Figure 21. Aniline.	17
Figure 22. Electrochemical polymerization.	18
Figure 23. Proposed mechanism for PANI. ⁷²	19
Figure 24. Polyaniline oxidative states.	19
Figure 25. PANI base to salt and delocalization mechanism.....	20
Figure 26. UV-Vis of PANI in solution, reacted at different temperatures. ⁸⁴	22
Figure 27. Carbon materials graphene, and graphene oxide.....	23
Figure 28. Formation of Mn_2O_7 from $KMnO_4$. ⁸⁵	24
Figure 29. (a) FTIR of GO^{96} and (b) Raman comparison between GO and graphite. ⁹⁷	25
Figure 30. Nucleation and growth of PANI nanowires GO sheets. ⁹⁸	26
Figure 31. (a) FTIR, and (b) UV-Vis of GO, PANI, and PANI-GO composite. ⁹⁸	27
Figure 32. SEM of (a) GO sheet, and (b) PANI-GO composite. ⁹⁸	27
Figure 33. (a) CV of GO, PANI, and PANI-GO composite, and (b) specific capacitance of PANI and PANI-GO. ⁹⁸	28
Figure 34. PANI doped with DSS (DSPA).....	30
Figure 35. Secondary doping of DSPA with m-cresol and thymol which has an additional alkyl branch.....	31
Figure 36. Drop casting method for DSPA films.	32
Figure 37. Dip coating method for DSPA films.	32
Figure 38. Vacuum filtration film prep for GO and rGO.	34

Figure 39. ^1H NMR of Aniline.	35
Figure 40. ^1H NMR of DSS	36
Figure 41. ^1H NMR of DSPA. Inset highlights the aromatic chemical shifts.	36
Figure 42. Optical image of DSPA _T in solution.	37
Figure 43. Optical image of DSPA _X in solution.	37
Figure 44. DSPA _T absorbance curves.	38
Figure 45. DSPA _X absorbance curves.	39
Figure 46. Absorbance curves of DSPA _X , ^m C DSPA _X , and ^{thy} DSPA _X .111	39
Figure 47. Prevention of secondary doping.	40
Figure 48. Conformational change induced via annealing.	40
Figure 49. DSPA _X film UV-Vis spectra.	41
Figure 50. ^m C DSPA _X film UV-Vis spectra.....	41
Figure 51. ^{thy} DSPA _X film UV-Vis spectra.....	41
Figure 52. SEM images of films (a) DSPA _T , (b) DSPA _X , (c) ^m C DSPA _X , and (d) ^{thy} DSPA _X	42
Figure 53. Picture of DSPA bulk films.	43
Figure 54. FTIR of as purchased graphite.	44
Figure 55. FTIR of GO from the first synthesis.....	45
Figure 56. FTIR of GO from the second synthesis.	46
Figure 57. FTIR of heat treated GO.....	46
Figure 58. FTIR of thermally reduced GO.	47

Figure 59. Picture of graphite and GO materials sonicated in H ₂ O, taken immediately after sonication and a 24 hour period.	48
Figure 60. (a) Ungrinded GO particles and (b) grinded GO particles.	48
Figure 61. ΔHGO and rGO suspended solutions over 24 hours.	49
Figure 62. UV-Vis of (a) ΔHGO and (b) rGO.	49
Figure 63. Optical microscopy of graphite particles.	50
Figure 64. Optical microscopy of ΔHGO particles at 0, 12 and 24 hours.	51
Figure 65. SEM of ΔHGO films.	52
Figure 66. SEM of rGO films.	52

LIST OF ABBREVIATIONS

APS	ammonium persulfate
C.E.	counter electrode
COP	chemical oxidation polymerization
CP	conductive polymer
CSA	camphorsulfonic acid
CV	cyclic voltammetry
DBSA	dodecylbenzene sulfonic acid
DSPA	DSS doped PANI
DSS	dioctylsulfosuccinate sodium salt
ECP	electrochemical polymerization
ED	emeraldine
FC	fuel cell
FTIR	fourier transform infrared spectroscopy
GO	graphene oxide
HOMO	highest occupied molecular orbital
LED	leuco-emeraldine
LUMO	lowest unoccupied molecular orbital
<i>m</i> C	<i>m</i> -cresol
PANI	polyaniline
PCE	power conversion efficiency
PEDOT	polyethylenedioxythiophene
PEM	proton exchange membrane

PN	pernigraniline
PSC	polymer solar cell
<i>p</i> TSA	<i>p</i> -toluenesulfonic acid
PV	photovoltaic
R.E.	reference electrode
rGO	reduced graphene oxide
SC	supercapacitor
SEM	scanning electron microscopy
thy	thymol
UV-Vis	ultraviolet-visible
W.E.	working electrode

CHAPTER 1. INTRODUCTION

1.1 Rationale

The need for alternative energy increases as the demand for energy increases. As the world's population continues to rise carbon emissions are expected to have a theoretical irreversible effect on the planet unless green sustainable energy solutions are found. Carbon emissions and greenhouse gases threaten the environment with global warming.¹ There is a desire within the United States as well as in the global community to encumber carbon emissions and stabilize the planet's climate. This is facilitated by the Clean Air Acts of 1990 and 2007, and the Kyoto Protocol which all aimed to place a cap on carbon emissions.^{1,2} It is shown, in **Figure 1**, that over 65 % of the world's energy is produced from oil, gas and coal.³ There is an alarming dependence on fossil fuels that have a substantial effect on the environment. A shift to renewable and sustainable energies needs to occur in order to reduce negative impacts. Current identified reserves of oil, gas and coal are expected to last for 41, 63 and 147 years respectively.⁴ The Shift Project reports that in 2014, 33 billion metric tons of CO₂ emissions were produced by the aforementioned sources of energy (**Figure 2**).⁵ Unfortunately, CO₂ emissions are projected to increase over the next several decades (**Figure 3**) as a result of energy demand.

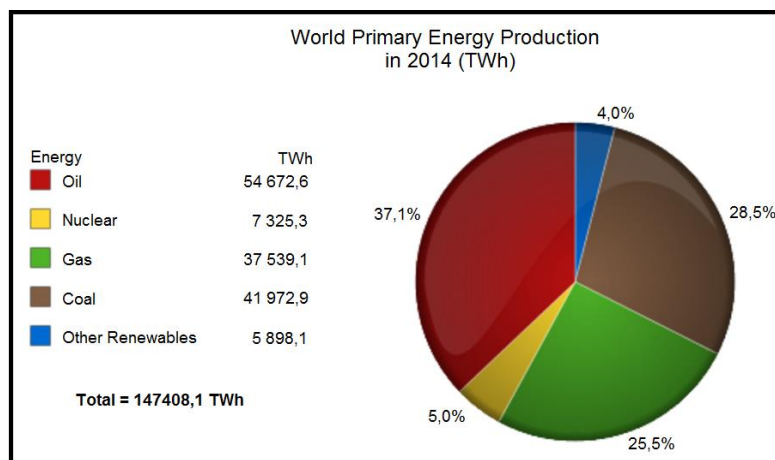


Figure 1. Electricity production by source.³

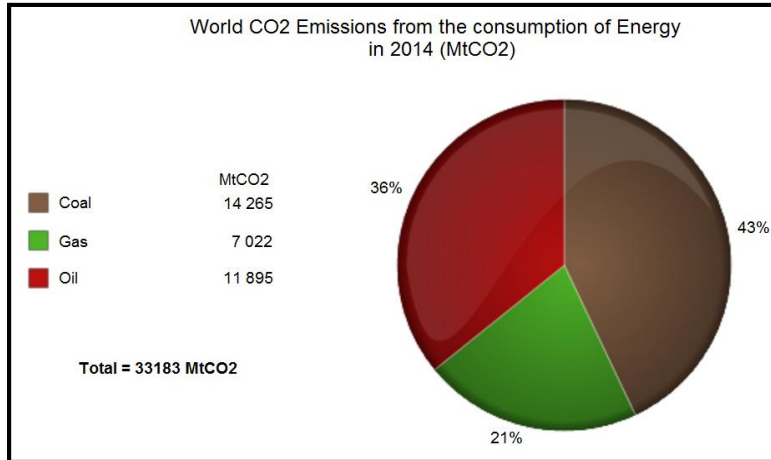


Figure 2. CO₂ emissions from energy consumption.⁵

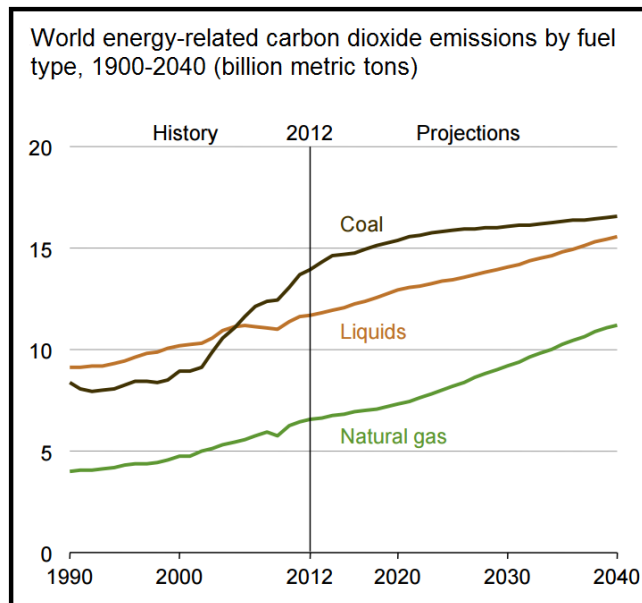


Figure 3. CO₂ emissions by fuel type.⁶

However, there is hope to reach the achievement of phasing out energy sources like coal, despite it being the cheapest and most abundant source of energy.² Similarly, oil is expected to have a smaller role in meeting energy needs. Despite contributing a smaller percentage overall oil consumption will increase. Presently, there is much investigation into many renewable energy technologies and sources such as photovoltaic (PV) cells, fuel cells and biofuels. Through sustainable energy practices climate should become more stable yielded a positive result on the global environment.

1.2 Electrically Conductive Polymers and Their Energy Applications

Various devices for energy conversion or storage can often include polymeric materials. A polymer is a large molecule made up of repeating units called monomers, connected by covalent bonds.⁷ The structure and properties of polymeric materials can change depending on the monomers and architecture of the polymer chain. Homopolymers consist of only one type of monomer unit while copolymers may contain two or more monomer units. **Figure 4** illustrates some of the different polymer chains that can exist in a copolymer system. Polymer chain architecture can vary from simple linear structures to more complex structures like extremely branched chains originating from a common core called dendrimers (**Figure 5**).⁸ The aforementioned components (monomers, homopolymer or copolymer, polymer chain architecture) are critical factors for determining and developing the application of synthesized polymers.

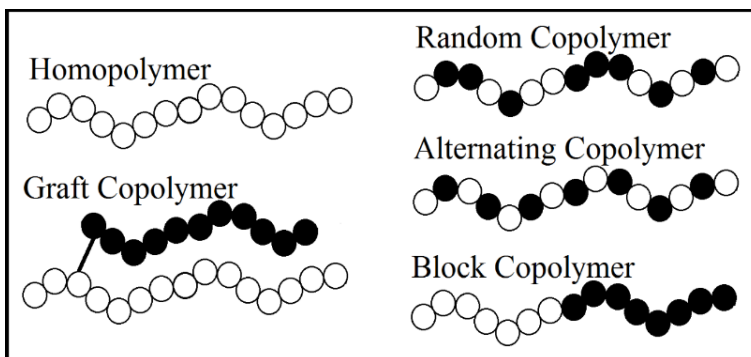


Figure 4. Homopolymer and copolymers.

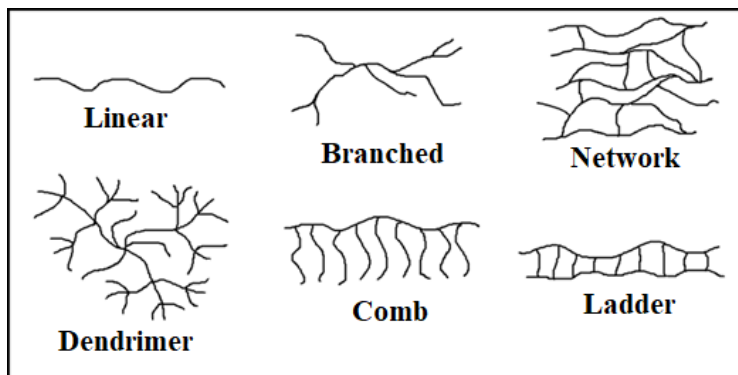


Figure 5. Polymer chain representations.⁸

Polymerization reactions commonly proceed through one of two approaches, step-reaction polymerization or chain-reaction polymerization. In a step-reaction polymerization, monomers combine randomly and are depleted hastily resulting in a low or moderate degree of polymerization.^{7,8} The polymerization depends on the amount of end groups left to react with each other. Chain-reaction polymerization requires an initiation to begin the process. Monomers are depleted at a slower rate resulting in higher degree of polymerization.^{7,8} **Figure 6** illustrates the basic mechanism between the two different polymerization techniques. Additionally, initiators are not only limited to chemicals such that polymerizations can be induced electrically by applying a potential. Different polymerization techniques, which are subsets of chain/step-reactions, have various effects on the polymer and can influence on the polymer through means of purity, degree of polymerization, molecular weight, stereoregularity, and contamination by the solvent or other added materials. The overall goal of polymerization is to synthesize a polymer free from defects and containing the desired mechanical, electrical, or optical properties. To achieve the highest quality polymers, syntheses have been established for certain polymers that minimize risk from defects and contamination, and maximize certainty of obtaining the chosen polymers and their associated properties.

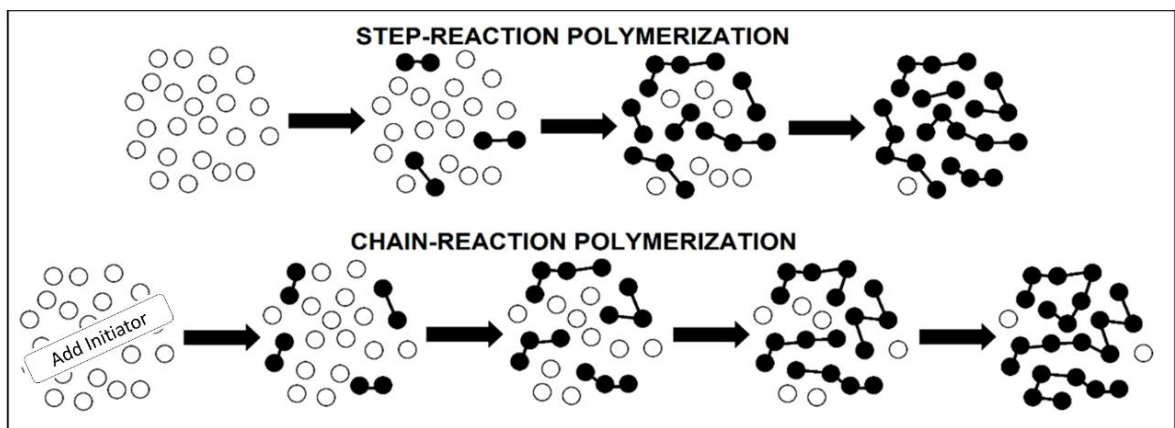


Figure 6. Polymerization mechanisms.

Electrically conductive polymers (CPs) are polymer molecules that possess the ability to transfer a charge within a conjugated system (alternating double/single-bond, **Figure 7**). Electrical conductivity is dependent on factors such as oxidation level, chain alignment, interchain interactions, and conjugation length as well as others.⁹ Even though they cover a broad range of conductivity (**Figure 8**), CP properties are not limited to electrical conductivity as their capabilities may also include ion-transportation, junction effects, and electrode effects.¹⁰ Additionally, there are many routes of synthesis to obtain a CP.¹¹

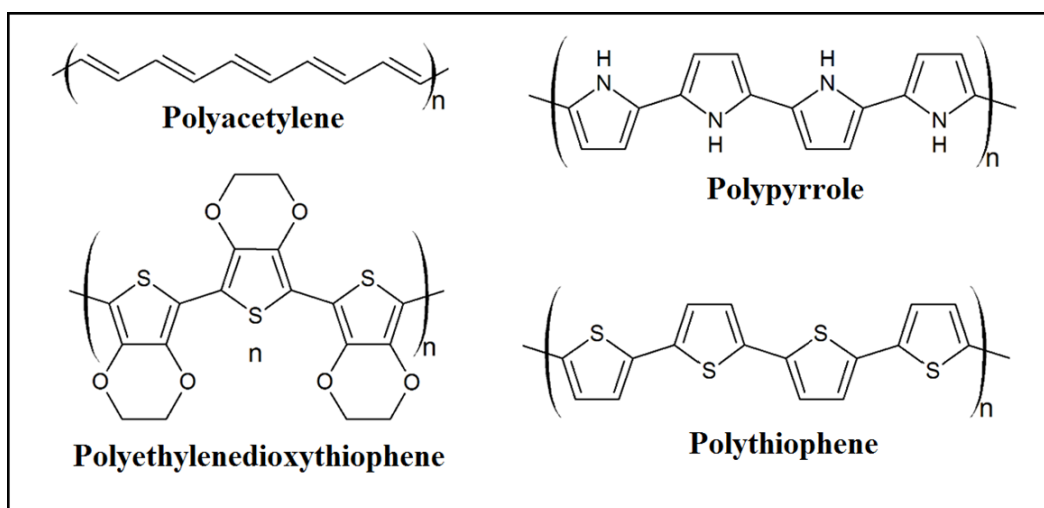


Figure 7. Electrically conductive polymers.

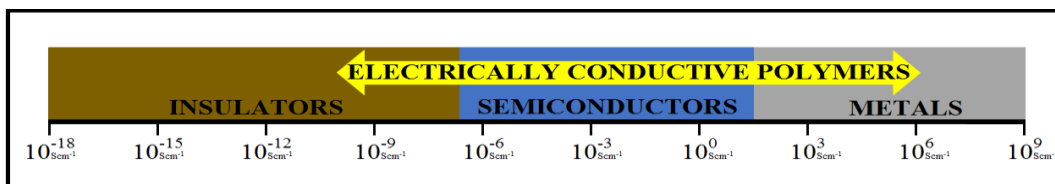


Figure 8. Conductivity of materials.

Charge transfer in CPs is accomplished through the delocalization of π -bond electrons in a conjugated polymer system as shown in polyethylenedioxythiophene (PEDOT), **Figure 9**.⁷ PEDOT has been used extensively in a broad range of devices that require charge transfer due to its characteristics in its highest occupied molecular orbital (HOMO) and lowest unoccupied molecular orbital (LUMO) levels also known as the energy band gap. As the spacing between these orbitals increase, as determined by the class of the material, more energy is required for electron transfer, **Figure 10**. It is ideal to reduce the spacing between HOMO and LUMO thereby reducing the amount of energy needed to promote conductivity. The charge mobility, μ_n , of the charged particles is determined by their velocity, V_d , across an electric field, E , in the equation:

$$\mu_n = V_d / E$$

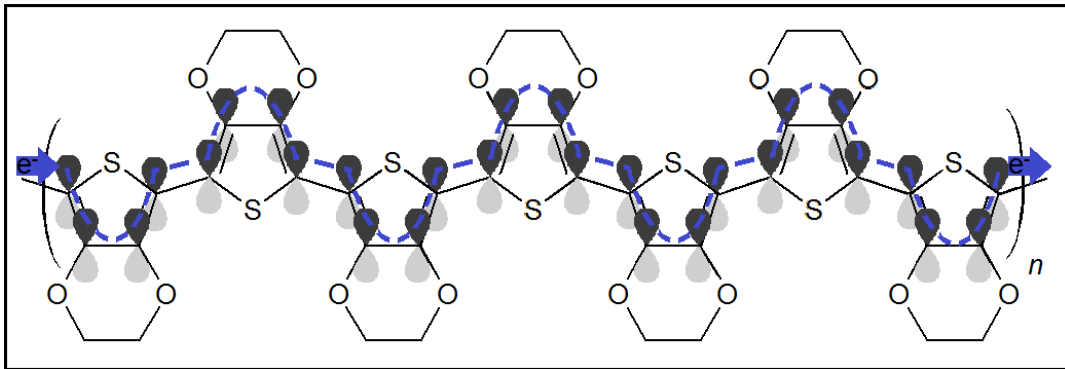


Figure 9. π -bond electron delocalization.

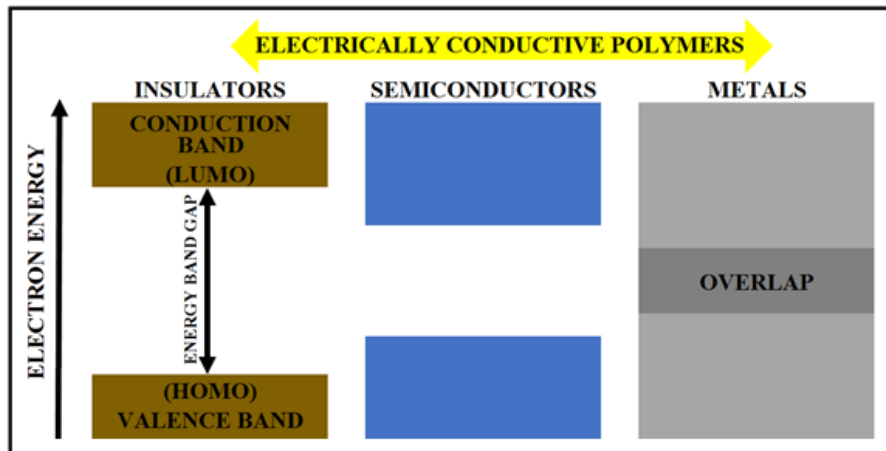


Figure 10. Energy band gap of materials.

Doping is very influential in the manipulation and control of conductive properties. Dopants can be any oxidation or reduction unit or an electron acceptor or electron donor unit that works to form charge transfer complexes creating delocalized radicals (**Figure 11**).^{8,11} Further effects of doping on the energy band gap are shown in **Figure 12**, where the dopants create new and smaller energy band gaps thereby increasing the conductivity of polymeric materials. Dopants can also induce a change in the polymer system from nonconjugated or partially conjugated to fully conjugated as is the case with polyaniline bases.¹² Some common methods of doping are gaseous doping, solution doping, electrochemical doping, and ion-exchange.¹¹ Doping is not only limited to the manipulation of conductive properties, it can also serve to improve the solubility of

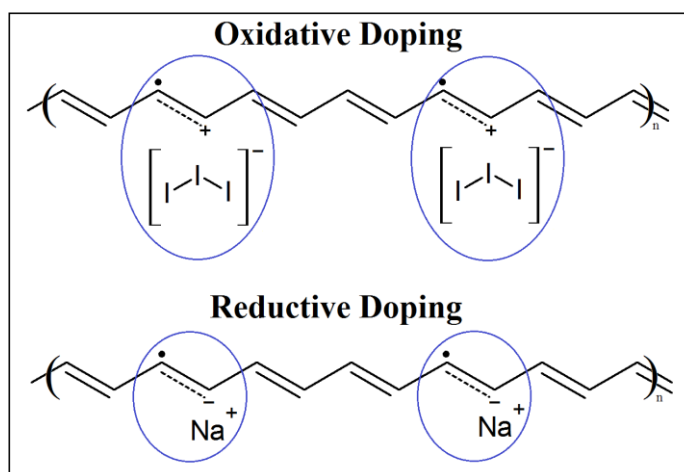


Figure 11. Charge transfer complexes formed from doping.

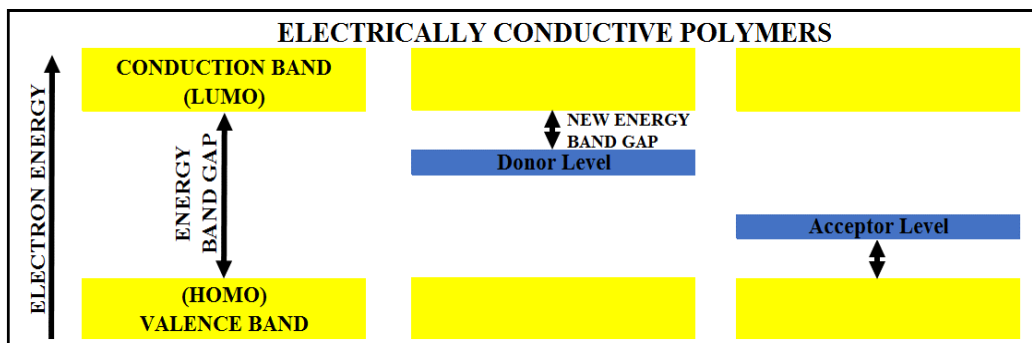


Figure 12. New energy band gap as the result of doping.

otherwise insoluble CPs. In so doing the configuration and crystallinity of CPs is altered which can produce negative or positive effects on electrical conductivity.⁸ Some common CPs, with their reported conductive range, are listed in **Table 1**. CPs are growing contributors in a broad range of conductive materials for energy storage and conversion devices.

Table 1. Some conducting polymers, their structure, conductivity, and type/doping.¹³

Polymer		Conductivity (Scm ⁻¹)	Type/Doping
Polyparaphenylene		500	n, p
Polythiophene		10-100	p
Polypyrrole		40-200	p
Polyisothianaphthalene		1-50	p
Polyaniline		1-100	p

1.2.1 Polymer Photovoltaic Cells

PV cells or solar cells are energy devices capable of converting photonic energy ($h\nu$) into electronic energy. The photoactive materials in these devices absorb sunlight which in turn excites electrons (excitons) and stimulates charge transfer between the HOMO and LUMO (**Figure 13**). The excited electron leaves behind a hole, and the pair requires formal dissociation with help from an applied electric field or materials that possess electron affinity.¹⁴ HOMO and LUMO energies can be calculated from the onset potential of oxidation and reduction versus the working electrode, E_{ox} and E_{red} respectively, shown in the following equations:¹⁵

$$\text{HOMO} = -e(E_{ox} + 4.38)(\text{eV})$$

$$\text{LUMO} = -e(E_{red} + 4.38)(\text{eV})$$

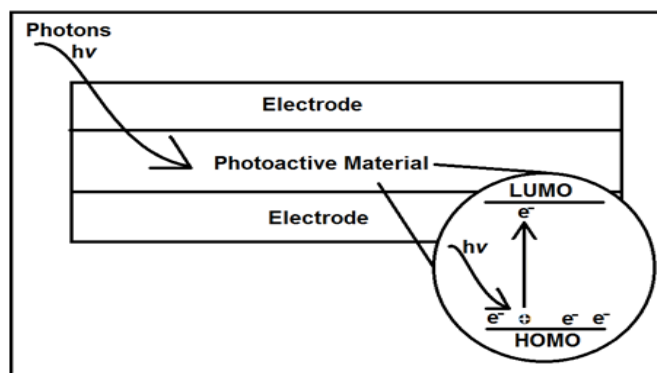


Figure 13. Solar cell schematic.

Polymer solar cells (PSCs) can be multilayer structures where each layer is fabricated individually (Krebs 2009).¹⁶ Interest in PSCs is the effect of the polymers' low-cost, lightweight, resource abundance, flexibility, and adjustable conductive properties.¹⁴⁻²¹ An adjustment of the polymer energy band gap to capture more photons can improve the short-circuit current density (J_{sc}).^{15,17,19,20} Furthermore, generation rate of excitons and the diffusion lengths of the respective excited electrons and holes ultimately determine J_{sc} . Additionally, decreasing the HOMO level and creating a narrower band gap can improve the open-circuit voltage (V_{oc}) thereby improving the power conversion efficiency (PCE) of PSCs.^{15,17,19,20} PCE is calculated as:

$$PCE = (V_{oc} J_{sc} FF) / P_{in}$$

where FF is the fill factor, calculated from J_{sc} vs V_{oc} curves, and P_{in} is the input power. Current PSCs have been able to achieve PCEs over 10%.^{14,15,19-21} Those PSCs were designed as multiple-junction tandem solar cells. Each junction works by absorbing at a specified wavelength then their efforts are combined forming a more efficient solar cell. **Figure 14** shows a tandem PSC fabricated by Riede et al., 2011 using the photoactive donor materials tetra-fluoro zinc phthalocyanine (F4-ZnPc), and α,ω -bis-(dicyanovinyl)sexithiophene)-Bu(1,2,5,6) (DCV6T), paired with the fullerene acceptor C_{60} and N,N'-diphenyl-N,N'-bis(4'-(N,N-bis(naphth1-yl)-amino)-biphenyl-4-yl)-benzidine (DiNPB) or 9,9-bis[4-(N,N-bis(biphenyl-4-yl-amino)phenyl)-9H-fluorene (BPAPF) as

the hole transport layer. Tandem PSCs have garnered attention due to the improvement in PCE when compared to conventional PSCs. The combination of polymeric materials will continue to expand the field of photovoltaics.

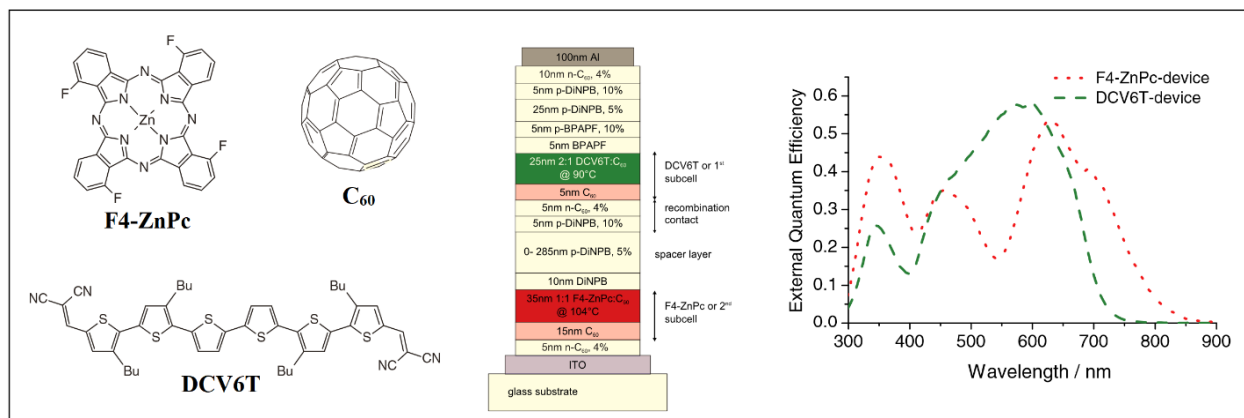


Figure 14. Chemical structure of the photoactive materials, stack structure of the tandem heterojunction device, and EQE spectra.¹⁹

1.2.1 Polymer Fuel Cells

A fuel cell is an electrochemical conversion device meaning that electricity is produced through chemical reactions.²³ It operates under the premise of taking in fuel and air then generating water, heat, and electricity as byproducts. More specifically, polymer electrolyte membrane or proton exchange membrane (PEM) fuel cells (FCs) transport hydrogen ions across its membrane in its production of electricity (**Figure 15**). The Dupont™ Nafion® membrane is a perfluorinated polymer and the most widely used PEM due to its high proton conductivity and excellent stability.²³⁻²⁶ The standard operating temperature for PEM FCs is between 50-100 °C, but most researched PEMs tend to lose efficiency when the temperature exceeds 100 °C.²⁷ However, research is trending towards more cost effective, environmentally benign and temperature stable polymers for these fuel cells.²⁴⁻²⁶

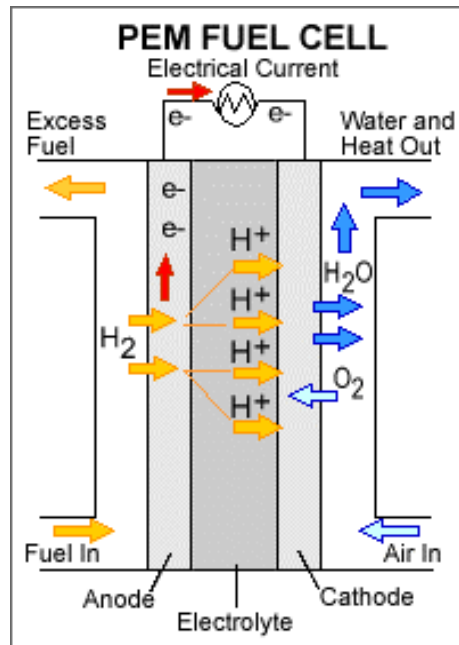


Figure 15. PEM fuel cell.²²

1.2.2 Polymer Ion Battery

In this electrochemical storage device, CPs can be applied as the positive electrodes called cathodes, or negative electrodes called anodes as shown in **Figure 16**.²⁷ Traditional batteries use CPs as the cathode with Li, Na, or Mg as the anode.²⁷ Typically, they exchange anions during the oxidation and reduction process called polymer doping/dedoping, where the anode is oxidized and the cathode is reduced.²⁸ The polymer electrode releases or collects ions to maintain electroneutrality and is an electronic/ionic conductor.²⁷ Important performance parameters for the CP electrodes are charge density, voltage difference to the counter electrode, coulombic efficiency, capacity, voltage efficiency, cycle life, self-discharge, and chemical stability.²⁷ Specific capacity, the measurement charge storage at a single electrode, is calculated from:

$$C_{\text{spec}} = (n \times F) / M_w$$

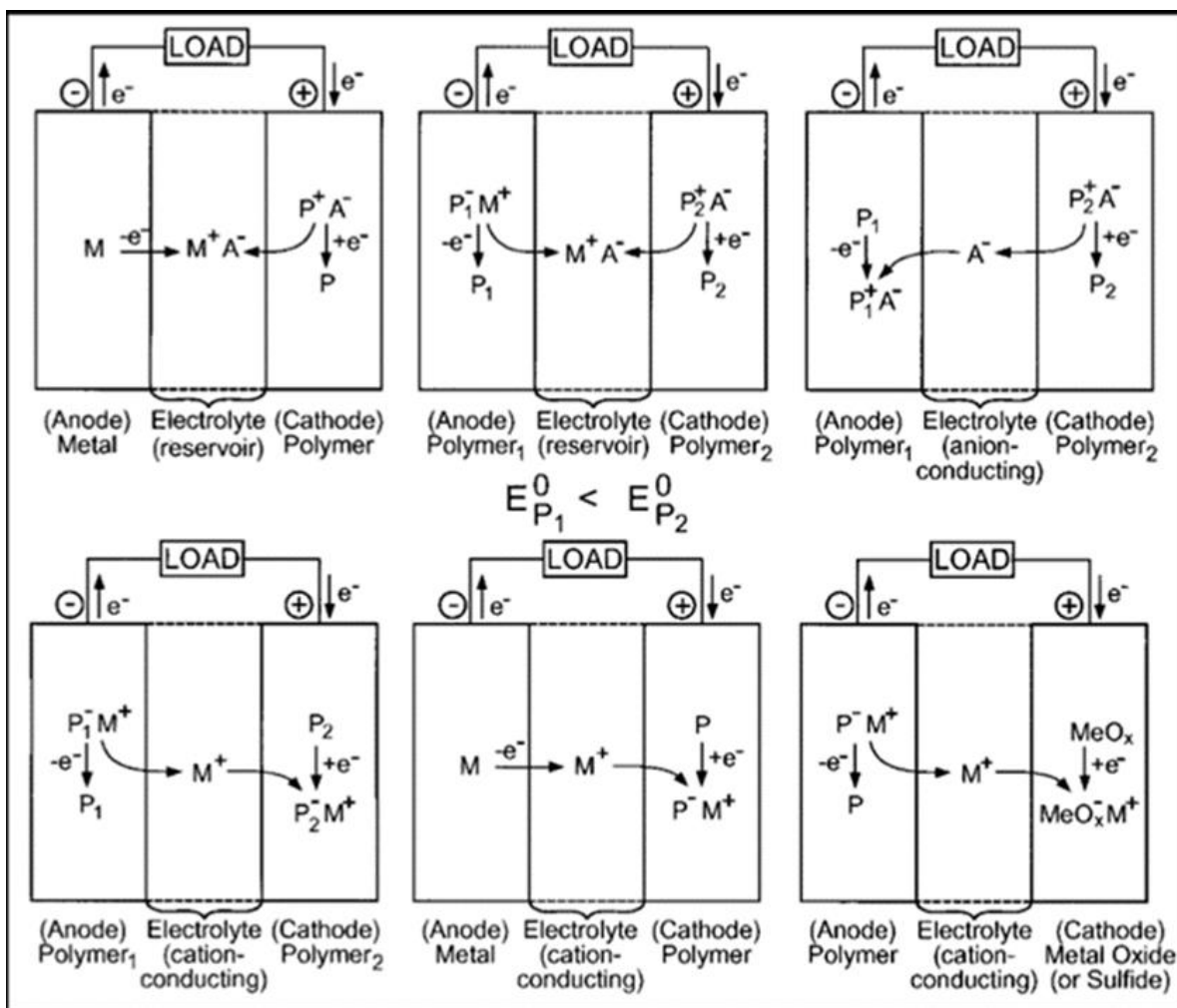


Figure 16. Schematic of CPs in cell assemblies. M stands for a metal, M+ for cations (typically metal ions), A- for anions, P for a neutral polymer, P- for a polymer in its reduced state, and P+ for a polymer in its oxidized state.²⁷

where n is the number of transferred electrons per redox reaction, F the Faraday constant, and M_w the molar mass of the structural unit.²⁸ The sum of C_{spec} of the anode and cathode is the total C_{spec} for the battery. Classification of battery cells depends on the reversibility of the redox reaction. Primary cells have a onetime use while secondary cells are rechargeable due to the reversible nature of their redox reactions. Unfortunately, batteries have only been able to reach 25-35% of their theoretical energy values.²⁸ **Figure 17** illustrates the different types of battery cells, with the cylindrical cell being the only battery not investigated with the addition of polymers.²⁸

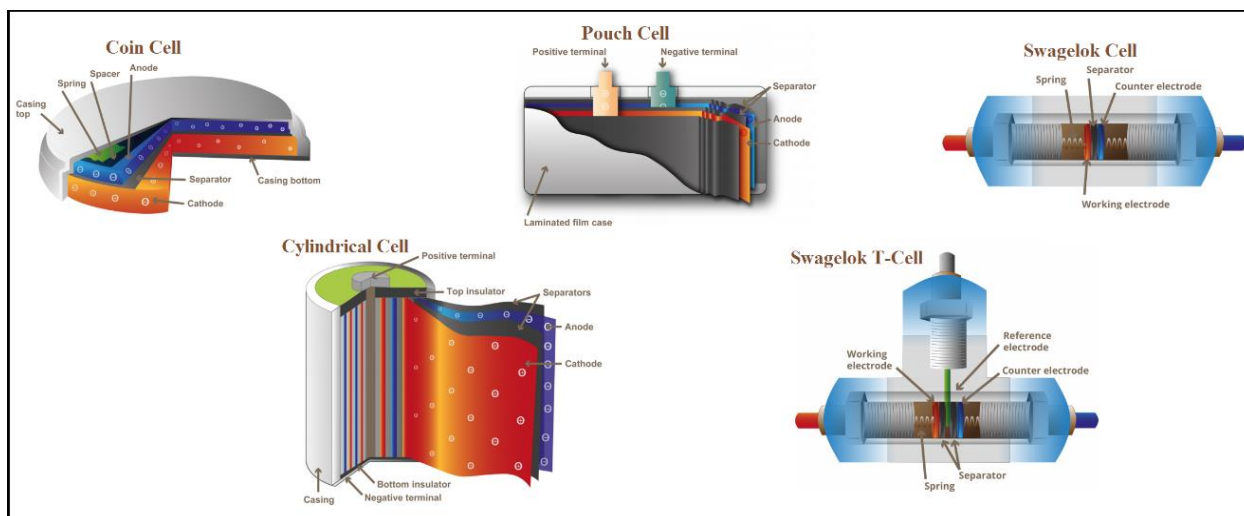


Figure 17. Schematic view of battery cells.²⁸

1.2.3 Polymer Supercapacitors

Supercapacitors (SCs) unlike batteries, boast fast charge/discharge rates, and are non-faradaic meaning they store charge through the physical adsorption and desorption of ions in porous carbon (Figure 18) rather than through redox chemical reactions. This physical charging storage mechanism allows for fast charge and discharge times and long life cycles.²⁹ Furthermore,

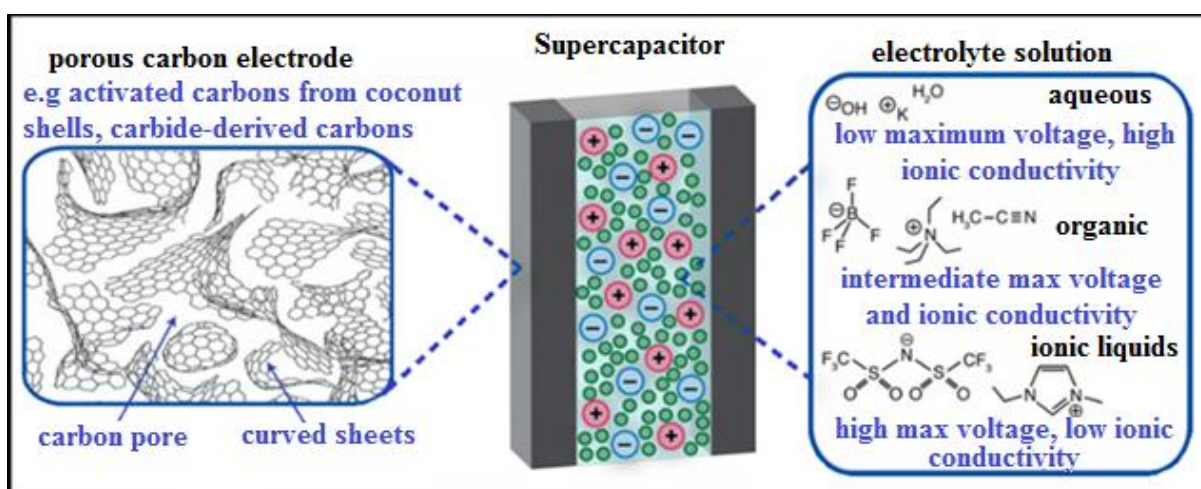


Figure 18. Schematic view of a SC. Porous carbon materials with disordered structures are used as the electrodes, and the cell is soaked with an electrolyte that maybe organic, aqueous, or ionic liquid-based, with some typical electrolytes shown.²⁹

an increase in energy reduces the power performance. Porous carbon materials are fabricated to increase the energy density thereby improving capacitance for energy storage. Specific energy density can be calculated from:

$$E = (1/2)C_{\text{cell}}V^2$$

where C_{cell} is the specific capacitance and V is the voltage.^{30,33} Furthermore the power density is calculated from:

$$P = E/\Delta t$$

where E is the energy density and Δt is the discharge time.³⁰ The porous carbon materials permit the charging mechanisms illustrated in **Figure 19**; the absorption of counter-ions, the counter-ion adsorption with counter-ion desorption called ion exchange, and counter-ion desorption. Regardless of the charging mechanism employed the excess ionic charge inside the porous carbon is equal and opposite to the electronic charge stored in the carbon.²⁹

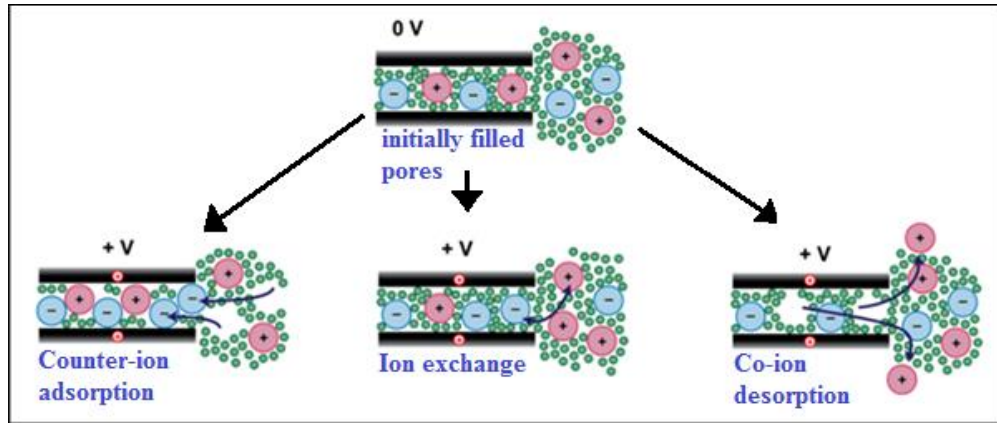


Figure 19. Charging mechanisms of SCs.²⁹

Polymeric materials have been incorporated into SCs as electrolytes, active electrodes, and carbon-polymer composite.³¹⁻³⁴ As electrolytes CPs demonstrate environmental safety while allowing for the development of flexible devices.³¹ They can exist as polymer gels which prevent electrolyte leakage. CPs can exhibit pseudocapacitive properties as electrodes at the interface with

the electrolyte consequently improving the energy density.³² More intricate materials are carbon-polymer composites as represented by Fan et al., 2014, **Figure 20**.³³ Through a multifaceted combination of materials, Fan et al., 2014 worked to develop a high-performance integrated electrode system. Pioneering models have incorporated photoactive CPs to prompt self-charging capabilities in SCs and innovation is still pressing forward.³⁴

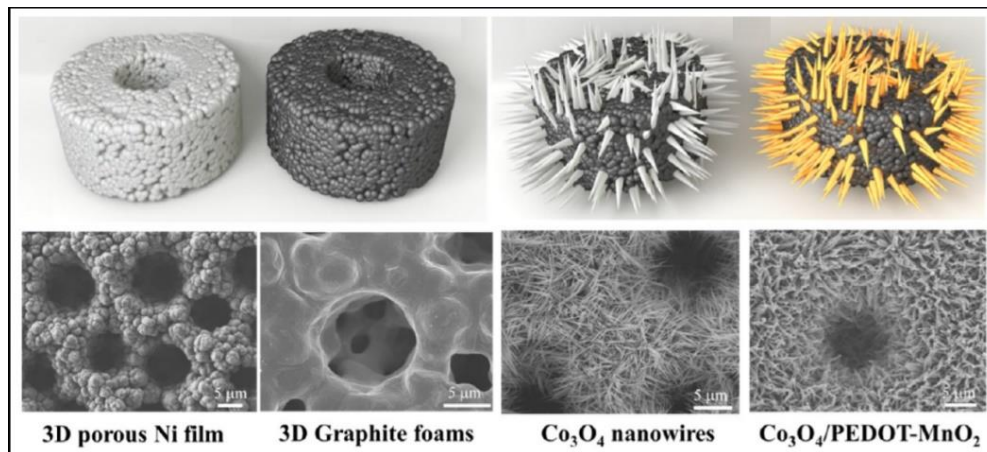


Figure 20. Schematics of the fabrication process of thin 3D porous graphite foams and their integrated composites.³³

Table 2. Polymer energy devices type and source.

Device	Polymer Materials	Energy Type	Energy Source
PSC	Electrodes, photoactive materials	Conversion	Photons
PEMFC	Electrolyte membranes	Conversion	Hydrogen Gas
Battery	Electrodes, electrolytes	Storage	Chemical redox reactions
SC	Carbon-composite electrodes, electrodes, electrolytes	Storage	Physical adsorption-desorption of ions

1.3 Thesis Objective

The purpose of this research project is to successfully synthesize polyaniline (PANI), graphene oxide (GO), and reduced graphene oxide (rGO) materials intended for the development of energy domains for energy storage/conversion. Carbon materials have been shown to produce synergistic effects in conjunction with conductive polymers. The development of materials to be incorporated in the energy device is arranged through the syntheses of organically soluble PANI and GO materials using an alternative modified Hummers' method. This is achieved through several steps:

1. The synthesis of solution processable PANI.
2. The fabrication of PANI film.
3. The synthesis of GO and thermal reduction to form rGO.
4. The fabrication of GO and rGO films.

CHAPTER 2. LITERATURE REVIEW

2.1 Polyaniline

Alan G. MacDiarmid may very well be considered a father of polyaniline (PANI) and CPs, because of his work beginning in the late 1970s, spanning almost three decades. He published articles on doping, synthesis, characterizations, and applications of PANI and other CP materials; he also owns several patents.³⁶⁻⁵⁴ Irrespective of his renowned works, PANI was discovered in the mid-19th century by physicians. However, their interest in aniline, **Figure 21**, was relegated to the investigation of poisoned coal workers and the of staining tissues for medical observation.⁵⁵ PANI was first reported in an electronic device in 1974 by Guinness, Corry, and Proctor.⁵⁶ Since that time PANI has become one of the most recognized CPs contributing to a broad range of energy devices.⁵⁷⁻⁶⁸

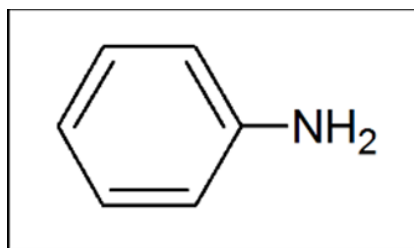


Figure 21. Aniline.

2.1.1 Synthesis of PANI

PANI is polymerized through a chain reaction polymerization initiated by an electrochemical method such as potentiostatic, potentiodynamic, and galvanostatic or an oxidative chemical including the common initiator, ammonium persulfate $(\text{NH}_4)_2\text{S}_2\text{O}_8$ (APS).⁶⁹ Electrochemical polymerization (ECP) requires the use of a working electrode (W.E.), counter electrode (C.E.), and reference electrode (R.E.). Electrons radicalize aniline at the C.E. and growth occurs on the W.E. as shown in **Figure 22**. ECP has the benefit of reducing the amount of

impurities in the PANI solution while granting control of initiation and termination steps.⁷⁰ Research has also been conducted studying the liquid-air interface during ECP and observing preferential orientations of PANI.⁷¹ Chemical oxidation polymerization (COP) requires the use of an oxidizing agent that consequently radicalizes the monomers thus beginning the polymerization process. As a free radical polymerization method, COP can proceed through many different

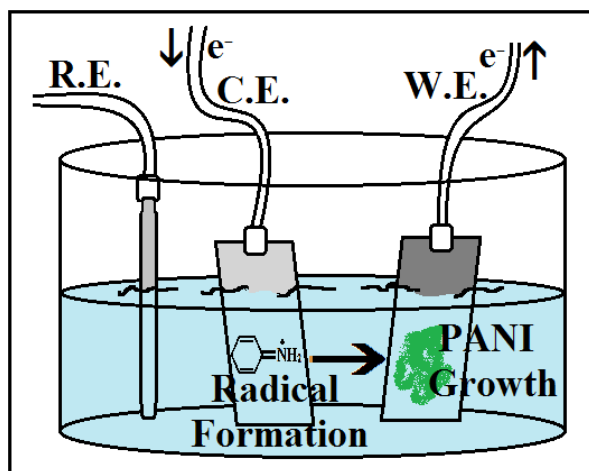


Figure 22. Electrochemical polymerization.

directions. COPs prohibit full management of initiation and termination, and can leave impurities within PANI that will obstruct conductivity. Consequently, many COP methods involve steps for the purification and concentration of PANI after synthesis. **Figure 23** illustrates a proposed mechanism for the radicalization, coupling, and propagation of aniline monomers to form dimers and oligomers.⁷² The carcinogen benzidine, although formed from a tail to tail coupling, is an infrequent occurrence at a high pH.⁷³

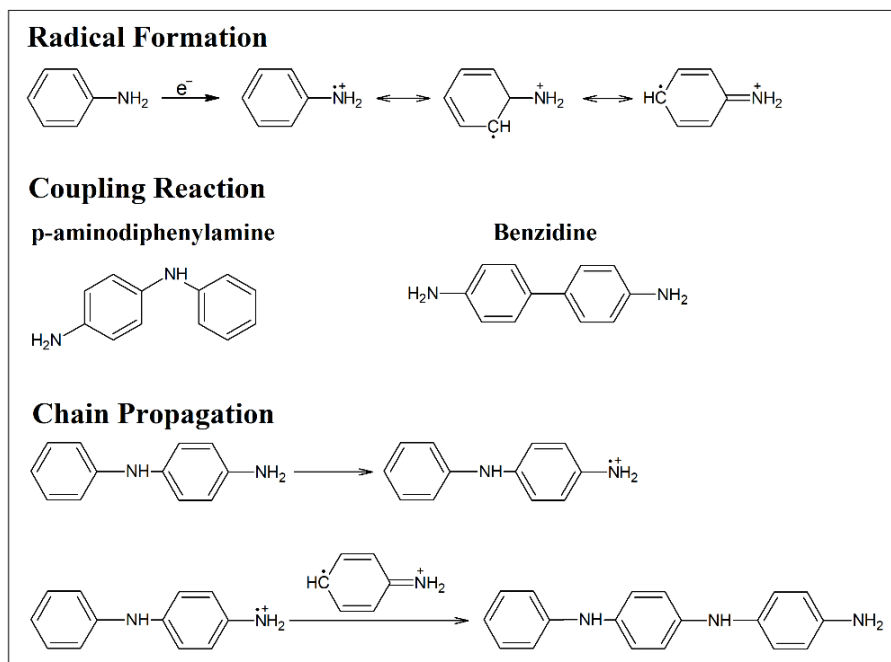


Figure 23. Proposed mechanism for PANI.⁷²

After polymerization, PANI will reach one of its oxidation states (**Figure 24**), from fully reduced leuco-emeraldine (LED) base to fully oxidized pernigraniline (PN) base with a half oxidized and half reduced emeraldine (ED) base between the two.⁷⁴⁻⁷⁶ The chromophores responsible for PANI's signature green color exist at the ED base, while the LED base has been reported as colorless and PN base has been reported as dark blue, purple, or black.

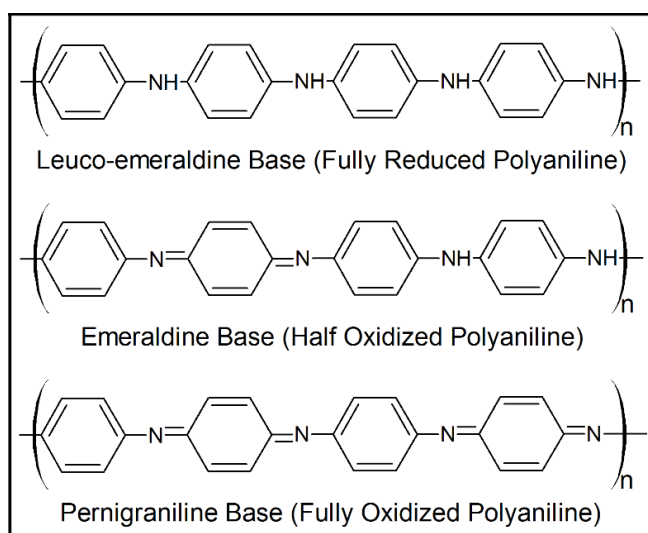


Figure 24. Polyaniline oxidative states.

2.1.2 Doping of PANI

In the base form PANI does not exhibit electrical conductivity and requires protonation, also known as doping, to achieve proper conjugation for electron delocalization to induce a charge.⁷⁷ Protonation occurs through treatment with an acid triggering a shift from PANI's base form to a new conjugated salt form.⁷⁸ Emeraldine salt delocalizes electrons from bipolaron to polaron for intramolecular charge transfer (**Figure 25**). In salt form the nitrogen-carbon bonds resonate between single and double bonds establishing an intermediate. Similarly, benzenoid and quinoid rings form an intermediate. The outcome is a highly conjugated π system.⁷⁴

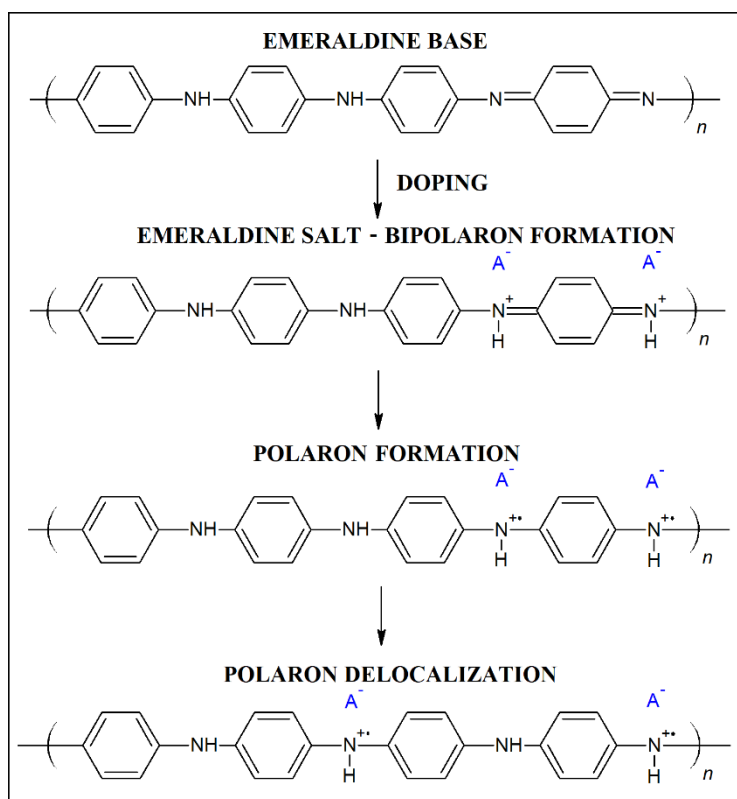


Figure 25. PANI base to salt and delocalization mechanism.

Doping of PANI is not only used to achieve improved conductivity, it is also used to influence the processability of PANI. Emulsion polymerization techniques include the use of dopants which are surfactants that contain functional groups contributing to enhanced solubility of

PANI.⁷⁹⁻⁸¹ They have been used to synthesis PANI in organic solutions such as toluene and xylene. Organically soluble PANI is beneficial for the development of PANI film and deeply affects the crystallinity. **Table 3** lists some common dopants for PANI and their desired impact.

Table 3. Common PANI dopants.

Dopant	Doping Stage	Impact
Camphorsulfonic acid (CSA)	During polymerization	Solubility
Diocylsulfosuccinate sodium salt (DSS)	During polymerization	Solubility
Dodecylbenzene sulfonic acid (DBSA)	During polymerization	Solubility
Hydrochloric Acid (HCl)	During polymerization	Conductivity
Hydrofluoric Acid (HF)	During polymerization	Conductivity
<i>m</i> -Cresol (<i>m</i> C)	During polymerization/after polymerization	Conductivity
<i>p</i> -Toluenesulfonic acid (<i>p</i> TSA)	After polymerization	Conductivity/ Solubility
Sulfuric acid (H ₂ SO ₄)	During polymerization/after polymerization	Conductivity
Thymol (thy)	After polymerization	Conductivity

2.1.3 Characterization of PANI

PANI's green color is a good indicator of a successful synthesis. Ultraviolet-visible (UV-Vis) spectroscopy typically displays two distinct peaks in the ranges of 250-400 nm and 550-800 nm (**Figure 26**).^{70,72,81-83} The UV-Vis peaks correspond to redox characteristics of the conjugated PANI system with red and blue shifts as the result of doping. X-ray diffraction and scanning

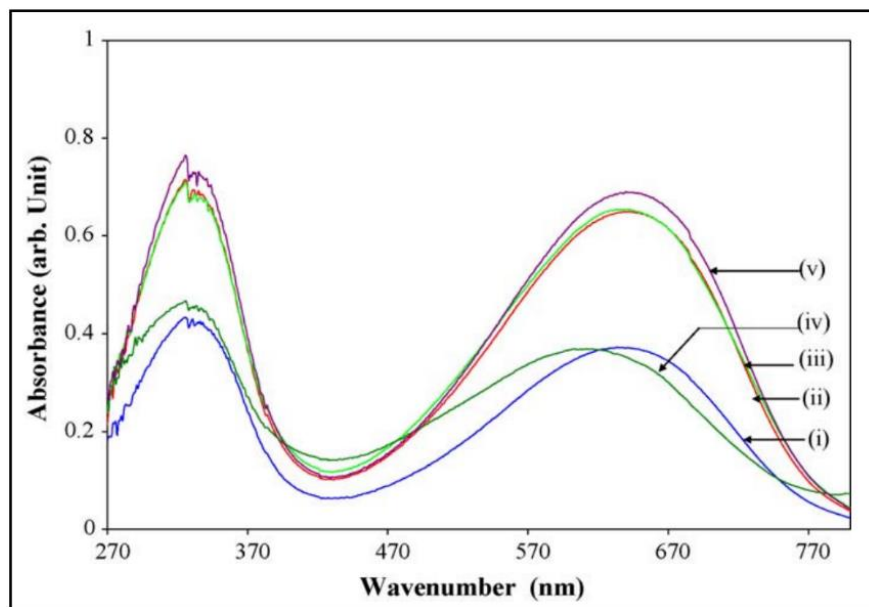


Figure 26. UV-Vis of PANI in solution, reacted at different temperatures (i:23.8 °C, ii:15 °C, iii:10 °C, iv:5 °C, and v:0 °C).⁸⁴

electron microscopy (SEM) of pure PANI materials show amorphous properties. PANI can have a broad range of conductivities, correspondingly cyclic voltammetry (CV) curves do not have any uniform redox peaks. Instead CV curves depend on the synthesis methods, whether chemical or electrochemical techniques were used, the quantity of dopants, and reaction time are some factors that will have an impact on the shape of the graph.

2.2 Graphene Oxide

Graphite, graphene, and graphene oxide (GO) are special carbon materials, **Figure 27**. Graphite, stacked layers of graphene, is the most abundant source of carbon. Graphene and GO possess unique conductive properties due to their conjugated structures. Conductivity of GO is dependent upon sp^2 hybridization. Therefore, GO can lose conductivity, becoming an insulator material, if it is over oxidized causing majority of hybridized orbitals to belong to the sp^3 regions. The oxygen functional groups make GO a suitable material for use in electronic devices because it is hydrophilic, easily dispersed, simple to functionalize, and possesses deposition methods less complicated than graphene.⁸⁵⁻⁸⁸ GO is derived from graphite starting materials and was first described in 1855 in a synthesis known as the Brodie method.⁸⁵⁻⁸⁷

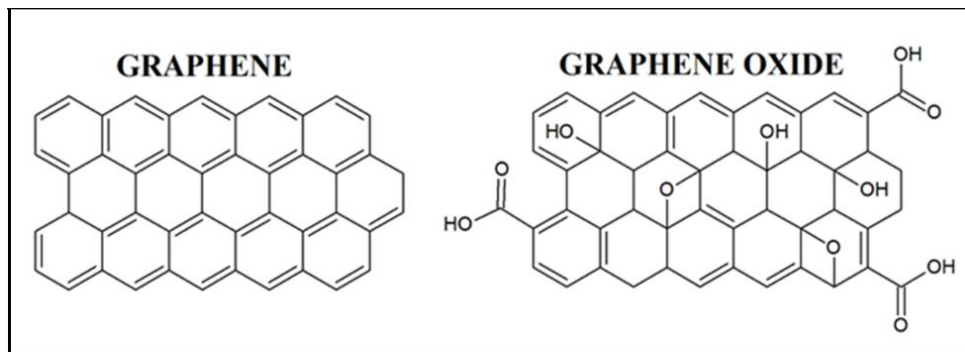


Figure 27. Carbon materials graphene, and graphene oxide.

2.2.1 Synthesis of GO

There are three well known synthesis methods for the production of GO; they are Brodie, Staudenmaier, and Hummers.^{85,86} Of the three, the Hummers' method is the most prevalent in modern GO materials research. However, the mechanisms of GO synthesis are not fully understood.⁸⁵ Nonetheless there are many variations to the original Hummers' method synthesis which aim to modify the oxidation levels of graphite, and improve the yield and quality of GO products.⁸⁹⁻⁹⁵

The Hummers' method uses potassium permanganate (KMnO₄) as the oxidant to treat graphite, which is suspended in sulfuric acid (H₂SO₄) with sodium nitrate (NaNO₃).⁸⁵⁻⁸⁷ Diamanganese heptoxide (Mn₂O₇), formed from potassium permanganates interaction with strong acids (**Figure 28**), is the active species of the oxidation process.⁸⁵ Temperature control is relevant to successful oxidations as the reactions are highly exothermic. Oxygen functional groups allow for further modification or easy deposition for film production.⁸⁷

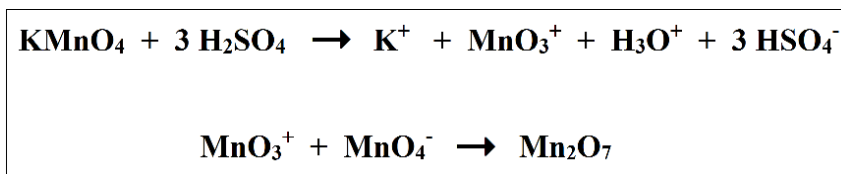


Figure 28. Formation of Mn₂O₇ from KMnO₄.⁸⁵

2.2.2 Characterization of GO

There are many ways to characterize GO to determine if the synthesis was successful. However, the vibrational spectra measured by **Figure 29 (a)**, fourier transform infrared spectroscopy (FTIR), and **Figure 29 (b)**, raman spectroscopy are clear indicators of achieved graphite oxidation. FTIR shows a broad range of O-H stretching between 3600-2400 cm⁻¹.⁹⁶ Alcohols, carboxylic acids, and residual water all contribute to the wide-ranging absorption peak. Carboxylic acid also contributes a C=O absorption peak at 1723 cm⁻¹.⁹⁶ The portion of FTIR spectra referred to as the fingerprint region, 1400-600 cm⁻¹, consists of overlapping vibrational modes.⁹⁶ In the raman spectra graphite shows a G band peak at 1578 cm⁻¹ and a weak D band peak at 1345 cm⁻¹. The G band corresponds to an E_{2g} mode of graphite and D band corresponds to A_{1g} phonon symmetry.⁹⁷ the G band and D band of GO shifts to 1588 cm⁻¹ and 1364 cm⁻¹ respectively, with the later increasing in intensity. I_D/I_G measures of the extent of disorder by indicating sp³ /sp²

carbon ratio.⁹⁷ Graphite has an I_D/I_G of 0.13 that increases to 0.88 for GO, signifying reduced sp^2 domains as a result of graphite oxidation.

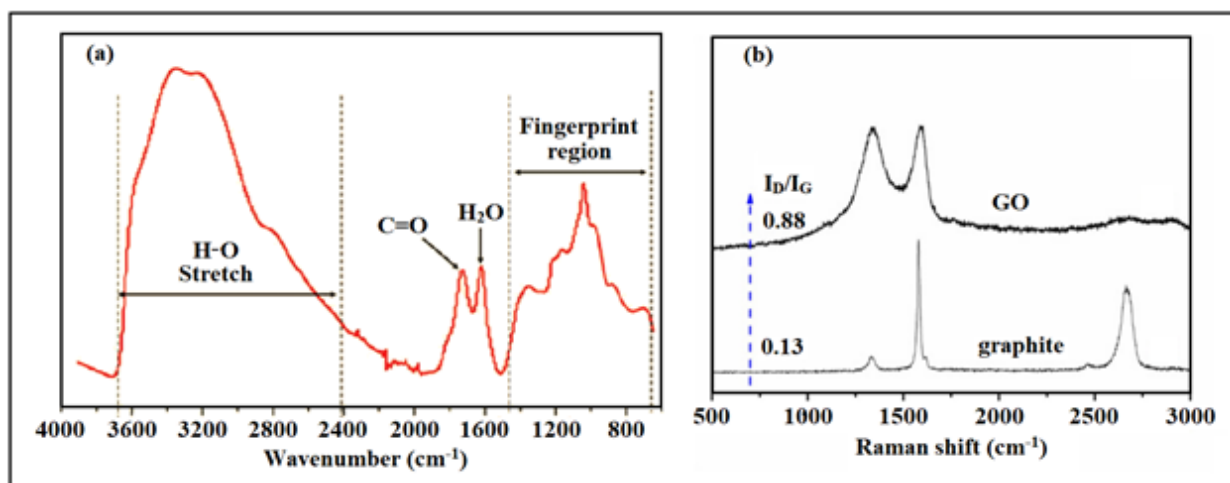


Figure 29. (a) FTIR of GO⁹⁶ and (b) Raman comparison between GO and graphite.⁹⁷

2.3 PANI-Oxide Energy Devices

As previously discussed the materials PANI and GO are good candidates for incorporation into energy devices. They can serve as individual layers or they can be blended to form composite materials. Through the adjustment of critical parameters between materials, such as weight/molar ratio, deposition method, size, architecture, and doping, optimal performances can be achieved. Furthermore, materials can sometimes exhibit synergistic effects, through a combined effort, greatly boosting device capabilities.

2.3.1 PANI Nanowires on GO for Energy Storage

PANI-GO nanocomposite material was synthesized by Wei et al for the purpose of inducing synergistic effects in the hierarchical structure. PANI was synthesized as nanowires arrays on 2D GO sheets (**Figure 30**). Highly-ordered nanostructure materials benefit device function by facilitating ionic interactions thereby, increasingly these materials are routinely incorporated in supercapacitors.⁹⁸

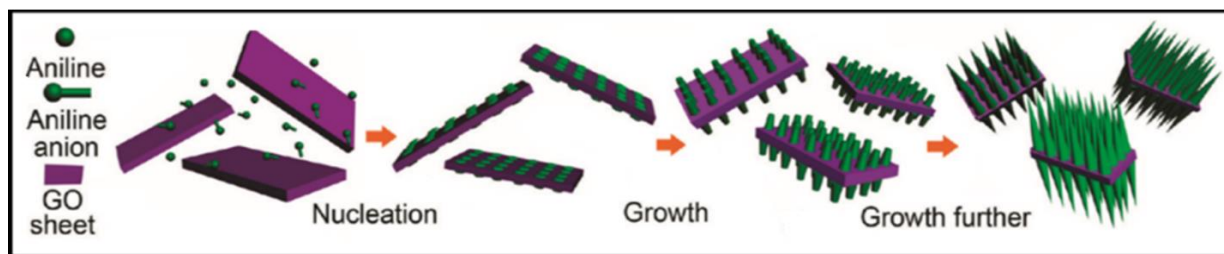


Figure 30. Nucleation and growth of PANI nanowires GO sheets.⁹⁸

GO was synthesized using the hummers method subsequently obtaining 2D sheets. **Figure 31 (a)** and **31 (b)** show the corresponding FTIR and UV-Vis for GO. The FTIR spectra of GO has signature peaks showing O-H, C=O, and H₂O at 3385, 1727, and 1635 cm⁻¹, respectively.⁹⁸ Additional peaks at 1405 and 1057 cm⁻¹ result from C-O stretching in alcohol and ether functional groups.⁹⁸ PANI was synthesized using COP with APS and nanocomposite material followed the same COP synthesis method in the presence of GO. PANI exhibits FTIR peaks near 1600 cm⁻¹ for C=N, 1500 cm⁻¹ for C=C, 1200 cm⁻¹ for C-N, and 750 cm⁻¹ for C-H bonds which appear in the resultant nanocomposite PANI-GO material. This indicates that the material was successfully merged without altering PANI and GO structure. UV-Vis spectra of PANI shows absorption at 450 and 800 nm which is consistent with typical absorption patterns and polaron transitions.⁹⁸ GO begins to show absorption towards the ultraviolet region typical of benzene ring spectra. The PANI-GO nanocomposite does not show a change in UV-Vis pattern. However, there is a decrease in absorption suggesting that the energy required for electron excitation has also been decreased.

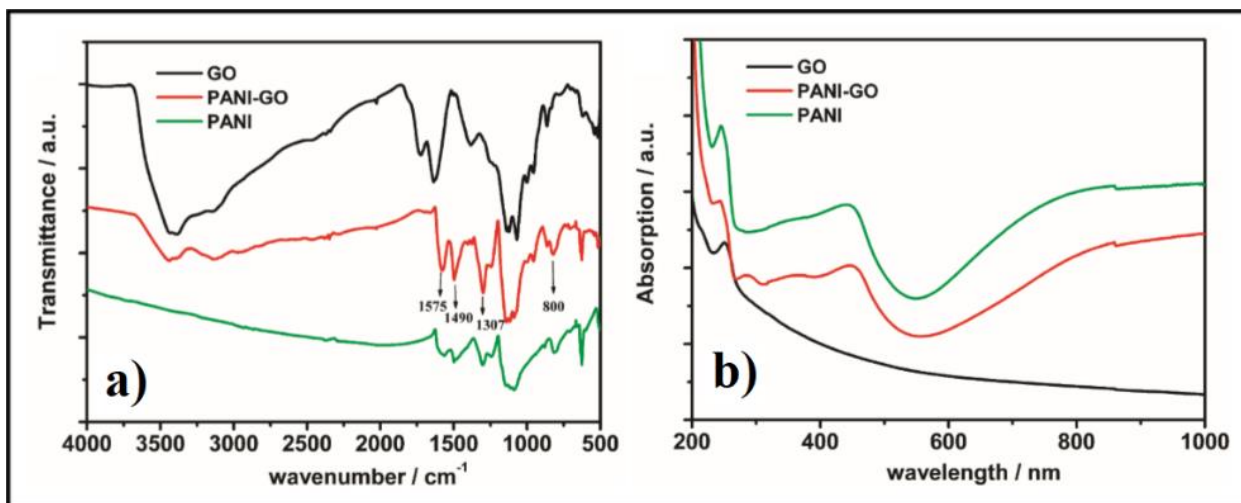


Figure 31. (a) FTIR, and (b) UV-Vis of GO, PANI, and PANI-GO composite.⁹⁸

SEM image, **Figure 32 (a)**, shows pristine 2D GO sheets of 20 nm thickness which is largely attributed to the gold deposition.⁹⁸ PANI-GO nanocomposite grown using the optimal concentration of 0.05 M aniline is illustrated in **Figure 32 (b)**. The 0.05 M aniline resulted in the creation of highly-ordered nanowire arrays.⁹⁸

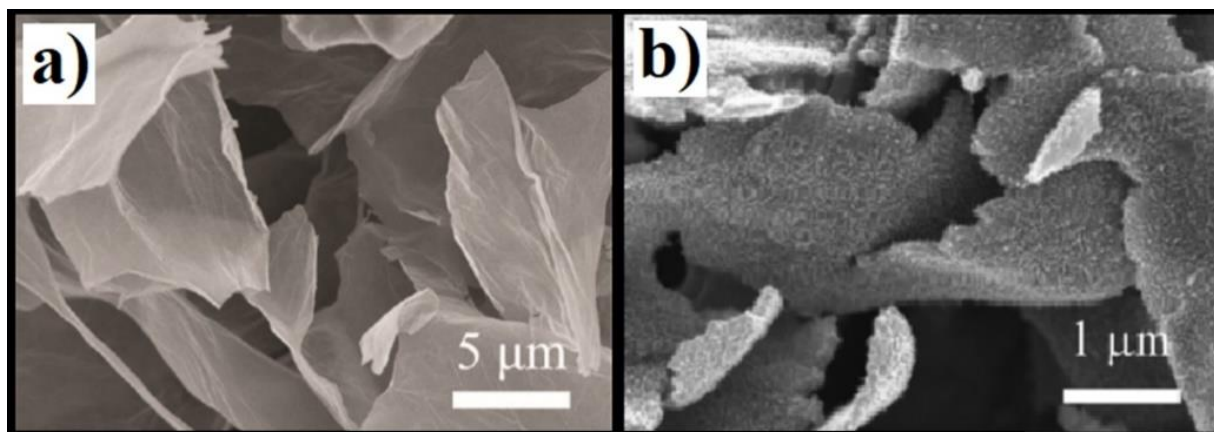


Figure 32. SEM of (a) GO sheet, and (b) PANI-GO composite.⁹⁸

The CV curves (**Figure 33 (a)**), for PANI-GO and PANI express two pairs of redox peaks which can be credited to PANI's transitions, LED-to-ED and ED-to-PN, with some enhancement for PANI-GO over pure PANI.⁹⁸ The specific capacitance (**Figure 33 (b)**) shows decreasing capacitance values as the current density increases for PANI and PANI-GO materials. However,

PANI-GO outperformed pure PANI at all current densities reaching a maximum specific capacitance of 555 F/g at the current density of 0.2 A/g.

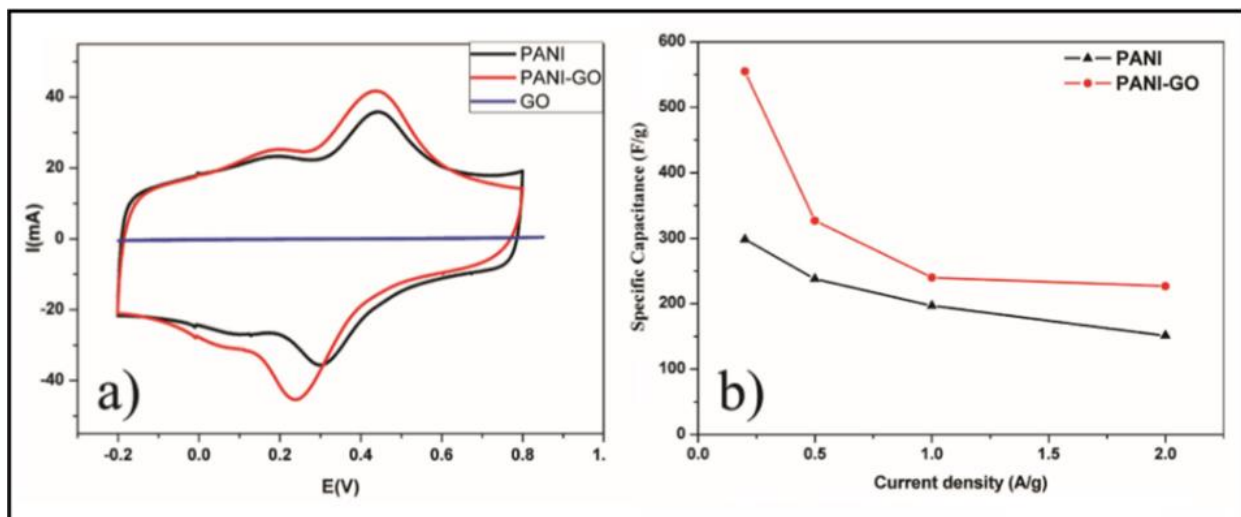


Figure 33. (a) CV of GO, PANI, and PANI-GO composite, and (b) specific capacitance of PANI and PANI-GO.⁹⁸

It is through optimization and the combination of materials that maximum capabilities can be reached. Previous factors mentioned, such as weight/molar ratio between materials and size dimensions, remain essential in developing the potential functions of composite materials. Resources are spent to combine materials in such a fashion that they reach the point of synergy. As demonstrated by Wei, this can be approached and achieved on the nanoscale, creating 2D nanocomposite material. Following this concept, the limitations of materials can be overcome by the synergistic effect.

CHAPTER 3. EXPERIMENTAL

3.1 Materials

Aniline, *m*-cresol, and thymol were purchased from Acros Organics. Dioctylsulfosuccinate sodium salt (DSS), 96%, was purchased from Acros Organics and Alfa Aesar. Pure powdered graphite was purchased from the General Pencil Company. Nomex[®] paper was received from the Dupont Company. Oxidizers potassium permanganate (KMnO₄) and sodium nitrate were purchased from Manofohm Chemical Supply Company and Loudwolf Industrial and Scientific, respectively. All water was obtained from a Millipore purifier (Q-Gard[®] 2). Other chemicals were purchased from Acros Organics, Fisher Scientific, Alfa Aesar, and LabChem Incorporated and used as received.

3.2 Characterization Equipment

Nuclear magnetic resonance (NMR) measurements were recorded on an Oxford NMR AS400 (EUR0034) with JEOL Eclipse 400 console. Chloroform-*d* with tetramethylsilane (TMS), from EMD Millipore, was the solvent for all NMR measurements and used to determine the composition of synthesized PANI. FTIR spectrophotometry measurements were taken on a Shimadzu IR Prestige-21 using KBr compressed pellets in a 10:1 weight ratio of KBr to sample, using 100 mg of KBr and used for the determination of successful oxidation of graphite. Optical properties and electronic transitions were examined by UV-Vis spectrophotometry on a Shimadzu UV-2450. UV-Vis spectra of PANI solution samples were prepared by diluting 10 μ L with 20 mL of solvent, PANI solid samples were prepared according to the drop casting method reported in section 3.5. UV-Vis spectra of GO solution samples were prepared by mixing 1 mg of GO with 20 mL of solvent after 1 hour of sonication in a Branson 1510 sonicator. Subsequent scans were recorded at 12 hour intervals up to 24 hours. A Nikon Eclipse Ni-U H550L captured all optical

microscopy images to illustrate dispersion of particles in solution. Samples were prepared using 10 μL of GO and PANI solutions on a glass slide. SEM images were taken by a Hitachi S-2600N to show size and morphology. Film samples were covered with gold. Conductivity was measured as surface resistance using a two probe Fluke 116 True RMS Multimeter with Pelco $\text{\textcircled{R}}$ conductive silver paint (Ted Pella, Inc.).

3.3 Synthesis of DSS Doped PANI

PANI was synthesized from a novel process. 35 g of DSS, in a 1.2:1 molar ratio of dopant:monomer, was combined with 127 g of H_2O and 27 g of 2-butoxyethanol then cooled under $5\text{ }^\circ\text{C}$. Then 6 g of aniline, cooled between $3\text{-}5\text{ }^\circ\text{C}$, was added to the solution and stirred for 1 hour. Next a precooled solution of 18 g of APS, in a 1.2:1 molar ratio of initiator:monomer, in 38 g H_2O was added over 30 minutes. The mixture was reacted for 8 hours under $5\text{ }^\circ\text{C}$ to form DSS doped PANI (DSPA). After the reaction 200 mL of *o*-xylene solvent was added to the mixture and separated. Finally, the mixture was washed, first with 77 mL of 1.7 mM H_2SO_4 solution and a second wash with 77 g of H_2O . A final 256 mL dark green polymer solution was obtained with 13 wt. % DSPA_X (**Figure 34**) that was subsequently increased to 15 wt. % via distillation. The synthesis was run a second using toluene as the organic solvent to obtain 156 mL of DSPA_T with 15 wt. %.

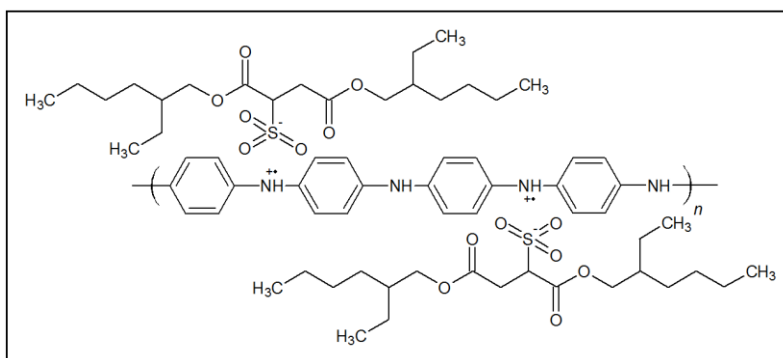


Figure 34. PANI doped with DSS (DSPA).

3.4 Secondary Doping of DSPA

Secondary doping of DSPA (**Figure 35**) occurred through in situ solution doping, after the polymerization was completed. The dopants, *m*-cresol and thymol, were added individually in a 5 % weight ratio to DSPA forming ^mC DSPA and ^{thy}DSPA.

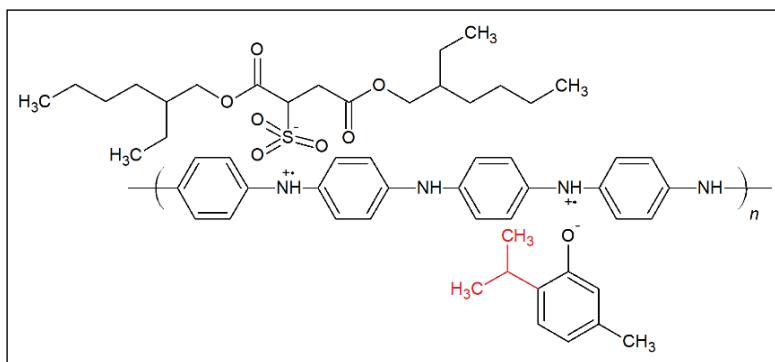


Figure 35. Secondary doping of DSPA with *m*-cresol and thymol which has an additional alkyl branch.

3.5 Fabrication of DSPA Films

DSPA films were produced via drop casting and dip coating. Both coating methods began with a preheated glass substrate from a BW Mechanical INC Precision incubator. The preheated substrates instigated better adhesion of the polymer to the glass surface. Prior to coating the DSPA solutions were sonicated for 5 minutes in a Branson 1510 sonicator.

The drop casting method (**Figure 36**) was executed by administering 20 μ L of DSPA solution to the substrate. The substrate was rotated to ensure broad distribution of DSPA over the surface. After the surface was covered and the polymer successfully adhered, excess polymer solution was drained off for characterization with UV-Vis. Subsequently, the prepared samples were air dried or heat treated at 130 $^{\circ}$ C for 60 minutes.

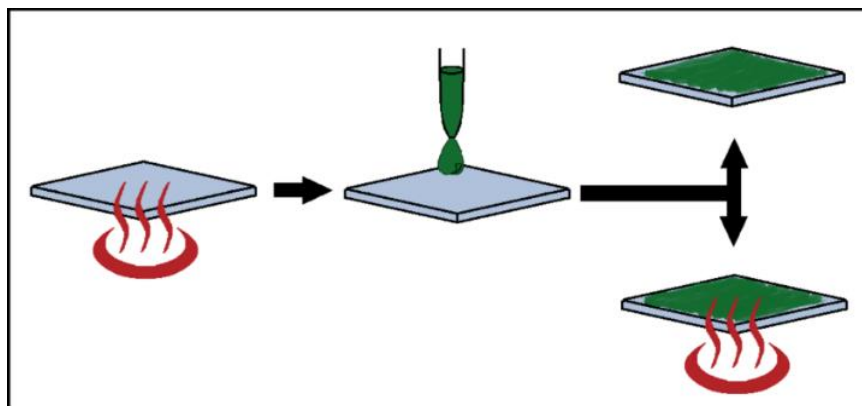


Figure 36. Drop casting method for DSPA films.

Dip coating (**Figure 37**) was achieved by carefully dipping the substrate into the polymer solution to the point of desired coverage. There was no delay in removing the substrate and all motions were smooth and free of irregular actions. Afterwards, the samples were placed on cellulose to remove the coating from the backside. Finally, samples were air dried or heat treated at 130 °C for 60 minutes.

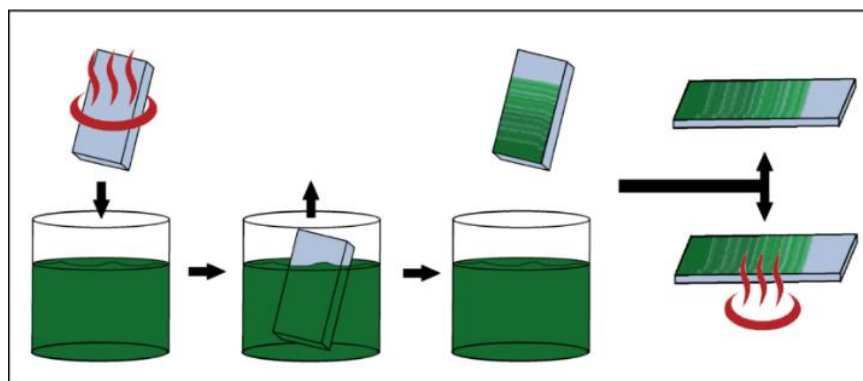


Figure 37. Dip coating method for DSPA films.

3.6 Synthesis of Graphene Oxide Materials

Synthesis of GO was modified from previous literature of an improved Hummers' method.⁹¹ 69 mL of concentrated sulfuric acid (H_2SO_4) was added to a mixture of 3.0 g of graphite powder and 1.5 g of sodium nitrate (NaNO_3). The mixture was then cooled using an ice bath to

<5 °C. Subsequently, 9.0 g of potassium permanganate (KMnO₄) was added slowly to prevent the reaction temperature from exceeding 20 °C. Next, the reaction was warmed to 35 °C and stirred for 7 hours. Then an additional 9.0 g of KMnO₄ was added in one portion, and the reaction was stirred for another 12 hours at 35 °C. The reaction mixture was then cooled to room temperature and poured into 400 mL of <5 °C water with 3 mL of 30% hydrogen peroxide (H₂O₂). After that the mixture was centrifuged at 4200 rpm for 1 hour, and the supernatant was decanted away. Then remaining solids were washed in succession with 200 mL of water, 200 mL of 30% HCl, and 200 mL of methanol, twice. For each wash, the mixture was centrifuged at 4500 rpm for 1 hour and the supernatant was decanted away. The remaining solid material was coagulated with 200 mL of petroleum ether and filtered using cellulose filter paper. The solid portions were obtained on the cellulose filter paper were dried overnight using a vacuum pump at room temperature resulting in 5 g of solid material. Obtained solids were ground into a brown powder and stored at room temperature. A second synthesis was run to include a pre-grinding step for the bulky graphite material. After synthesis solids were ground forming a tan powder. Upon heating under vacuum at 120 °C for 2 hours to remove residual water, a dark brown powder was obtained and stored at room temperature.

Reduction of GO occurred through thermal treatment. A temperature of 180 °C was applied for 1 hour under vacuum forming reduced GO (rGO). Powder was black in color and stored at room temperature.

3.7 Fabrication of GO and rGO Films

GO material films were fabricated on Nomex ® paper. The Nomex ® paper was placed inside a vacuum filter (**Figure 38**). Next, 3 mL of a sonicated GO solution was deposited on the substrate. The concentration of GO solutions was 1 mg mL⁻¹.

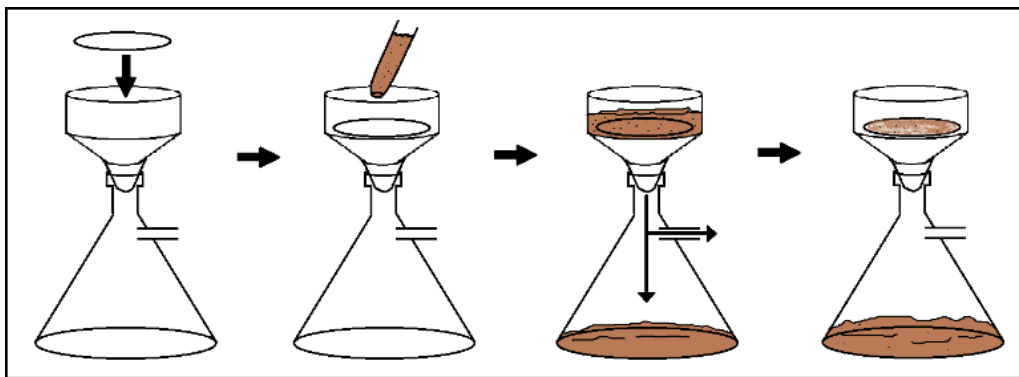


Figure 38. Vacuum filtration film prep for GO and rGO.

CHAPTER 4. RESULTS AND DISCUSSION

4.1 DSPA Characterization

Characterization methods for DSPA include proton (^1H) NMR, optical microscopy, UV-Vis, SEM, and surface resistance. ^1H NMR was used to determine the successful polymerization of aniline monomers with the attachment of the alkyl dopant, DSS. Similarly, UV-Vis was used to confirm polymerization through absorption patterns and indicate changes in the conformational arrangement of DSPA molecules.

4.1.1 DSPA ^1H NMR

Confirmation of DSPA synthesis is shown from ^1H NMR. The prominent peaks at 0 and 7.27 are solvent peaks for D-chloroform with TMS. Aniline, **Figure 39**, exhibits peaks corresponding to its benzene ring ranging from 6.6 to 7.2 ppm. There are two more peaks at 1.55 and 3.6 ppm, these variable peaks represent the amine group NH_2 . DSS (**Figure 40**) has primary,

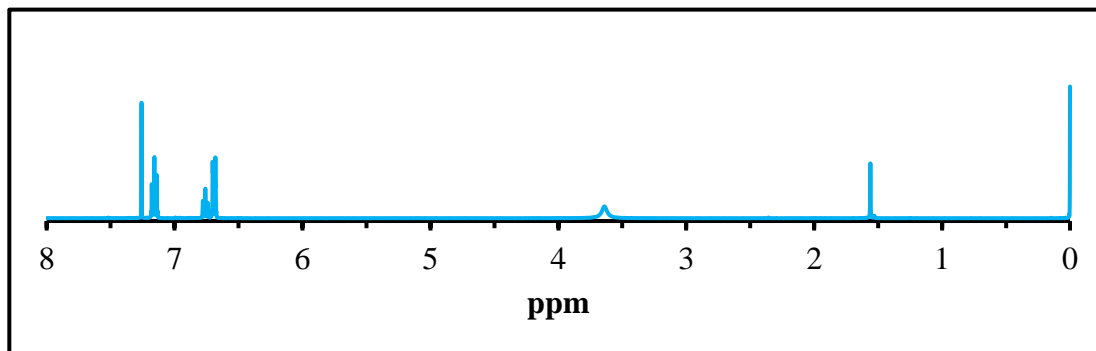


Figure 39. ^1H NMR of Aniline.

secondary, and tertiary alkyl groups which are consistent with the peaks at 0.86, 1.38, and 1.52 respectively. The ester functional groups in DSS display a very broad range of chemical shift peaks starting from 2 and continuing until 4.3 ppm. **Figure 41** shows ^1H NMR for DSPA in toluene and

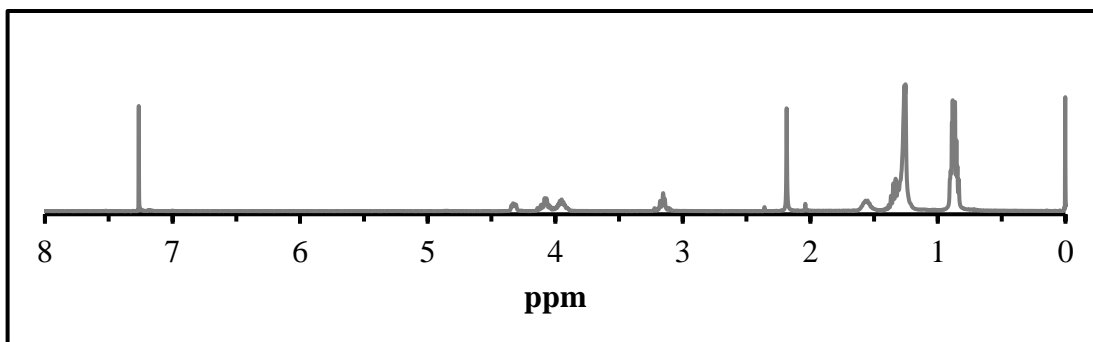


Figure 40. ^1H NMR of DSS

xylylene. The alkyl portions from DSS are easily identified as being attached to PANI thereby forming DSPA. Previous DSS peaks at 2.2 ppm have shifted and the corresponding ester and amine peaks between 3 and 4.5 are indistinguishable. Aromatic peaks, shown in the inset of **Figure 41**, do not show high intensity when compared to DSS contributing alkyl groups. The small peak at 9.3 ppm resembles SO_3H indicating that PANI may be over saturated with the dopant DSS.

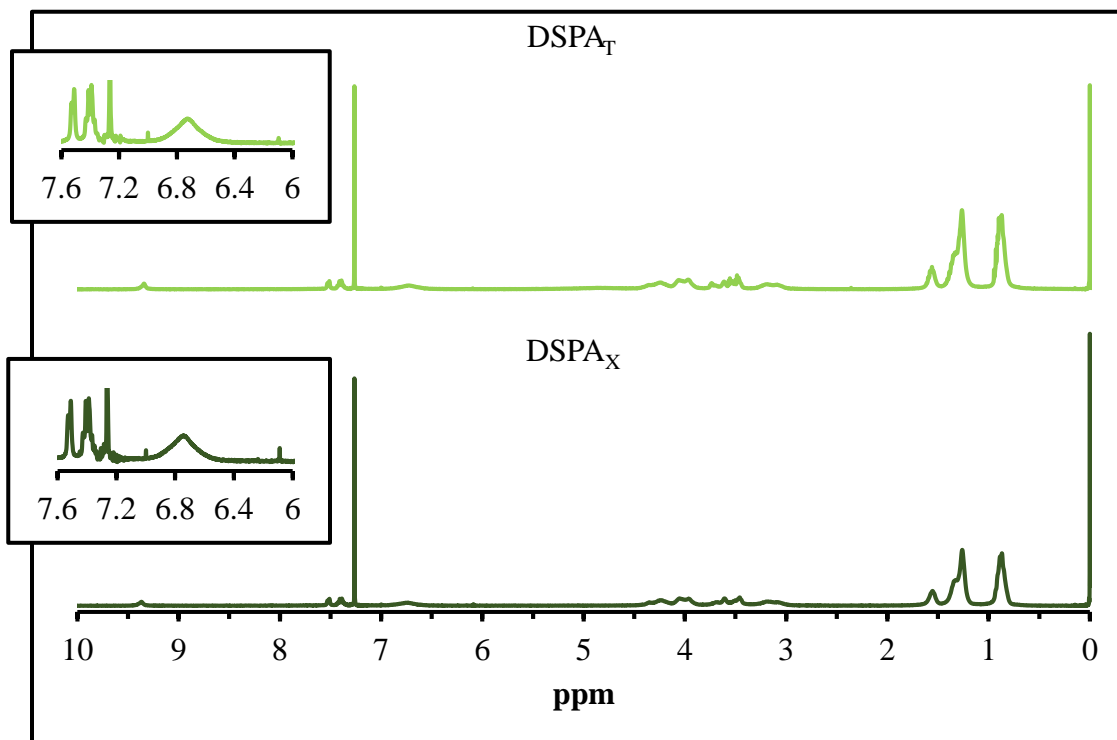


Figure 41. ^1H NMR of DSPA. Inset highlights the aromatic chemical shifts.

4.1.2 DSPA Solution Optical Microscopy

Investigation of DSPA solution with optical microscopy reveals that aggregation has occurred in both DSPA_T and DSPA_X with the later exhibiting more advanced aggregate formation, **Figure 42** and **43** respectively. DSPA_T and DSPA_X have similar amounts of over saturation with

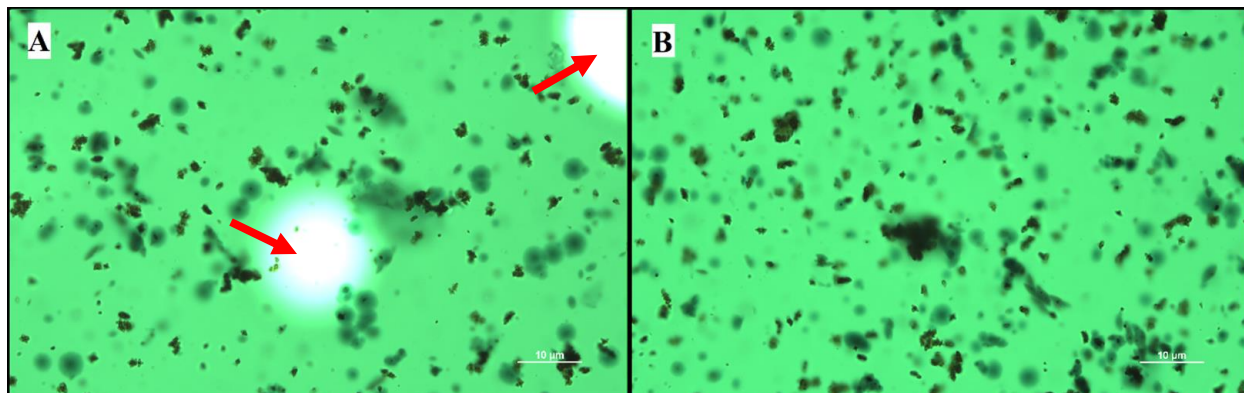


Figure 42. Optical image of DSPA_T in solution.

DSS, however *o*-xylene appears to cause a limitation in the amount of aggregates formed possibly due to the additional methane group. In addition to having excessive aggregation, DSPA_T has also displayed micelle formation pointed out by the red arrows in **Figure 43 (a)**. Excess DSS molecules may have formed these groups using SO₃H as the polar interior in toluene solution whereas *o*-xylene prevented micelle formation.

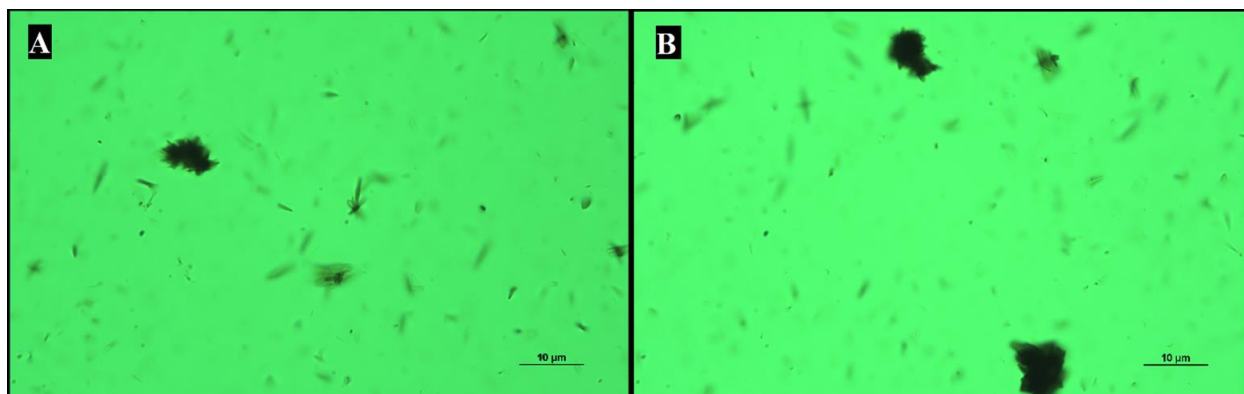


Figure 43. Optical image of DSPA_X in solution.

4.1.3 DSPA Solution UV-Vis Spectra

UV-Vis spectra analysis indicates that DSPA was successfully synthesized as the absorbance patterns are consistent with previous literature.⁸⁴ Although the absorbance patterns remain regular, DSPA solution products are not completely homogeneous. Multiple scans of DSPA_T yields significant gradated absorbance curves (**Figure 44**). DSPA_T UV-Vis spectra is influenced by the micelles and extreme aggregation observed in **Figure 42**. DSPA_X also showed aggregation, though less intense, in **Figure 43** subsequently, the UV-Vis spectra demonstrated

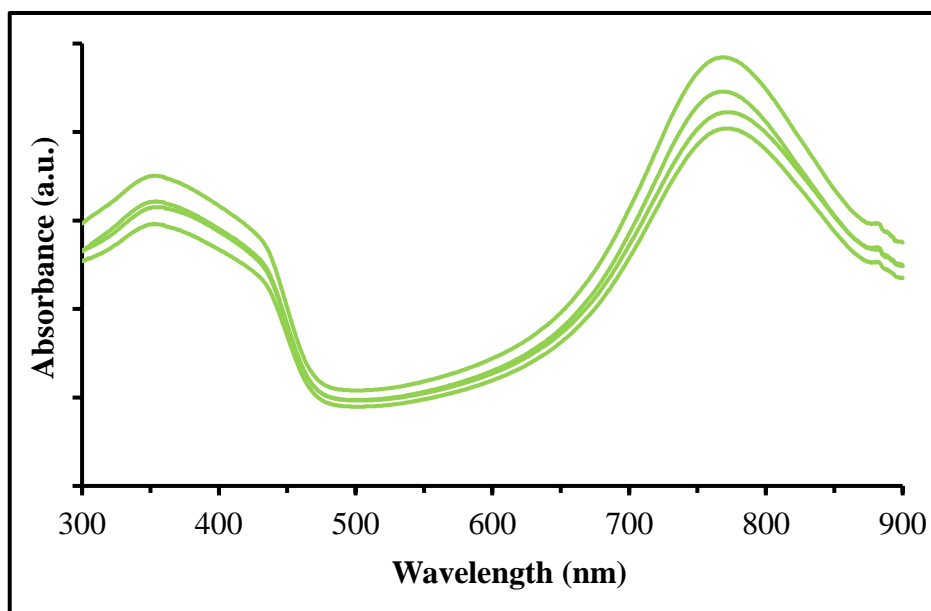


Figure 44. DSPA_T absorbance curves.

gradated absorbance curves in a more moderate form (**Figure 45**). Despite the scaling of absorbance curves of DSPA, redox patterns are observed. Therefore, the synthesized materials maintain the capability of transferring charge via excited electron. DSPA_X gives the impression it is the more suitable candidate for incorporation into charge transfer applications due to its increased dispersion and more reliable UV-Vis spectra.

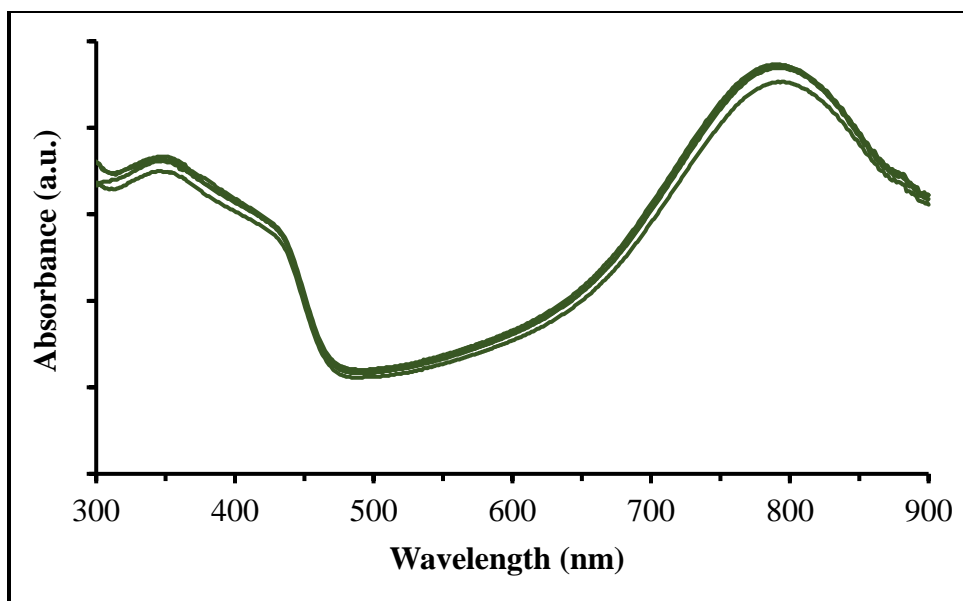


Figure 45. DSPA_X absorbance curves.

Considering DSPA_X's stable patterning with UV-Vis, doping was applied to DSPA_X solutions. The dopants, *m*C and thymol (thy), were used in 5 wt. % additions to DSPA_X. However, the UV-Vis spectra of *m*C doped DSPA_X (*m*^CDSPA_X) and thy doped DSPA_X (^{thy}DSPA_X) did not produce the anticipated results. The redox patterns of *m*^CDSPA_X and ^{thy}DSPA_X remained nearly identical to that of undoped DSPA_X (**Figure 46**) signifying no change to the polaron transitions.

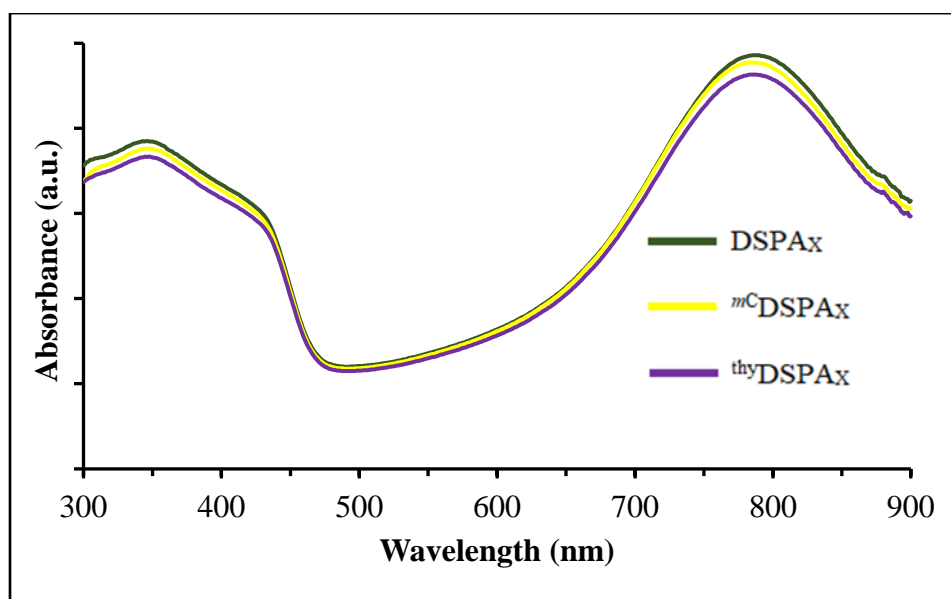


Figure 46. Absorbance curves of DSPA_X, *m*^CDSPA_X, and ^{thy}DSPA_X.

m^C DSPA_X and thy DSPA_X expressed absorbance curves similar to the gradated curves in **Figure 44** suggesting that the secondary doping was unsuccessful. Steric hindrance and site availability caused by the saturation of DSPA with DSS, **Figure 47**, are the likely obstructions that prevented effective secondary doping.

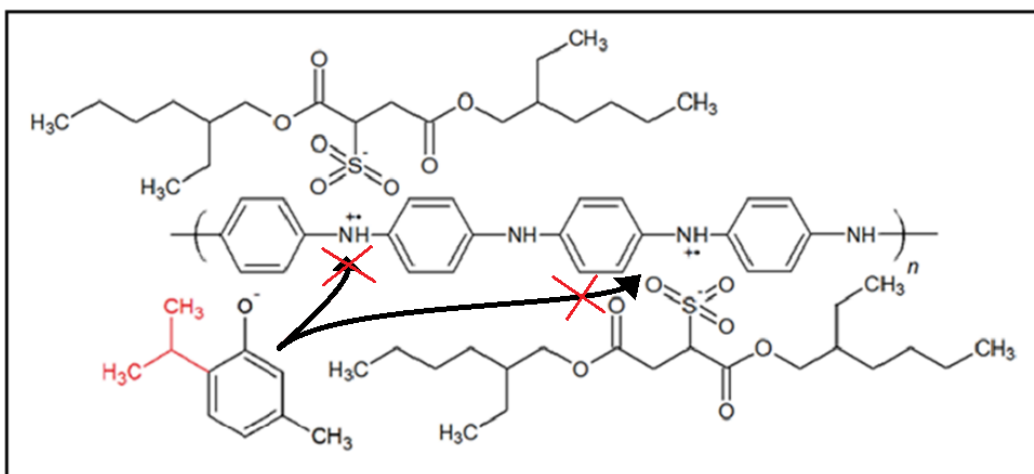


Figure 47. Prevention of secondary doping.

4.1.4 DSPA_X Film UV-Vis Spectra

Although secondary doping of DSPA_X appeared to be ineffective films were fabricated using DSPA_X, m^C DSPA_X, and thy DSPA_X. Annealing polymer films can induce a conformational change in the alignment of the polymer chains (**Figure 48**). Straightening the tangled polymer allows for tighter packing thereby improving charge transfer. DSPA_X, m^C DSPA_X, and thy DSPA_X films were

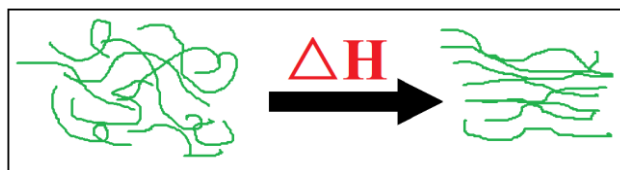


Figure 48. Conformational change induced via annealing.

annealed at 130 °C for 60 minutes and the results illustrated in **Figures 49, 50, and 51** respectively.

All films demonstrated some improvement in their alignment. Peaks corresponding to electron

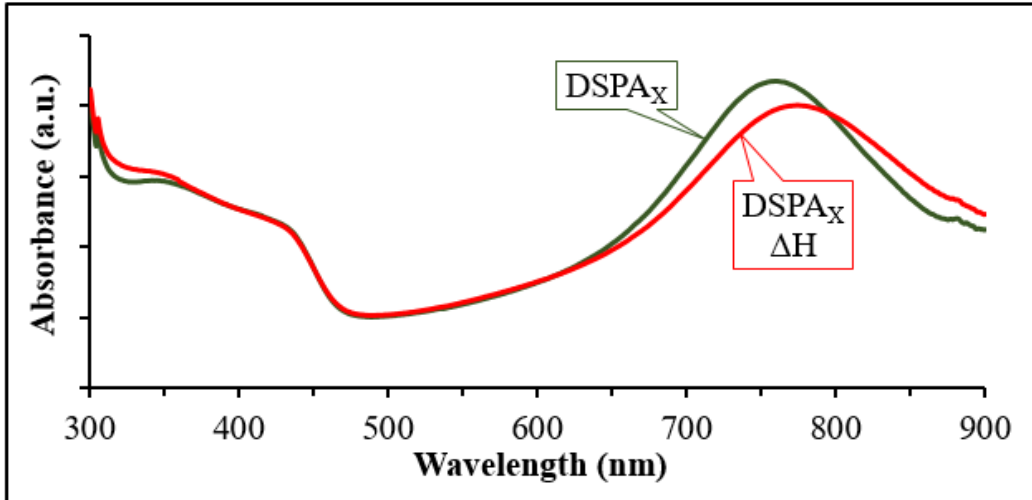


Figure 49. DSPA_X film UV-Vis spectra.

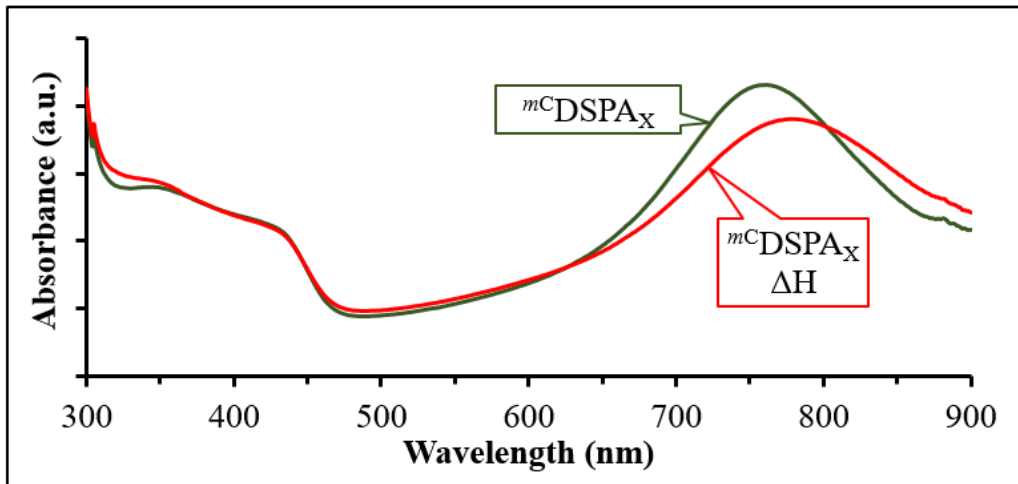


Figure 50. *m*^CDSPA_X film UV-Vis spectra.

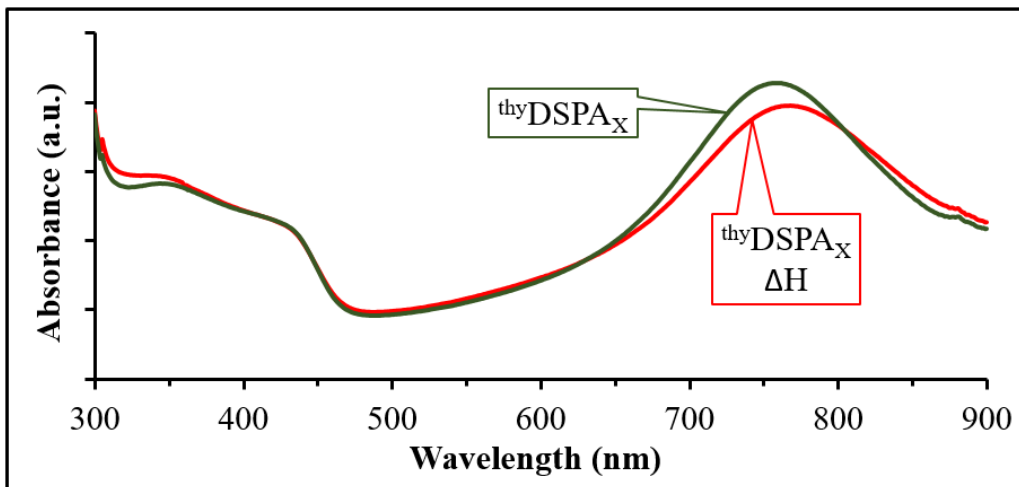


Figure 51. thy DSPA_X film UV-Vis spectra.

excitation were reduced. The reduction indicates a smaller energy requirement which further signifies a better adjusted configuration of DSPA molecules. Although **Figures 50** and **51** show that the added dopants did not exhibit any beneficial impact on the improved configuration it is important to note that the dopants did not exhibit any adverse effect on configuration.

4.1.5 DSPA_X Film SEM

Films were fabricated using DSPA_T, DSPA_X, ^mC DSPA_X, and ^{thy}DSPA_X. SEM of DSPA_T and DSPA_X exhibit a major dissimilarity in film formation (**Figure 52 (a)** and **52 (b)**). The micelles imaged in **Figure 43 (a)** resulted in major deformities in DSPA_T film. This deformation interrupts the charge transfer capability of DSPA_T. DSPA_X, ^mC DSPA_X, and ^{thy}DSPA_X films display similar characteristics, **Figure 52 (b)**, **52 (c)**, and **52 (d)** respectively. This is an expected outcome since

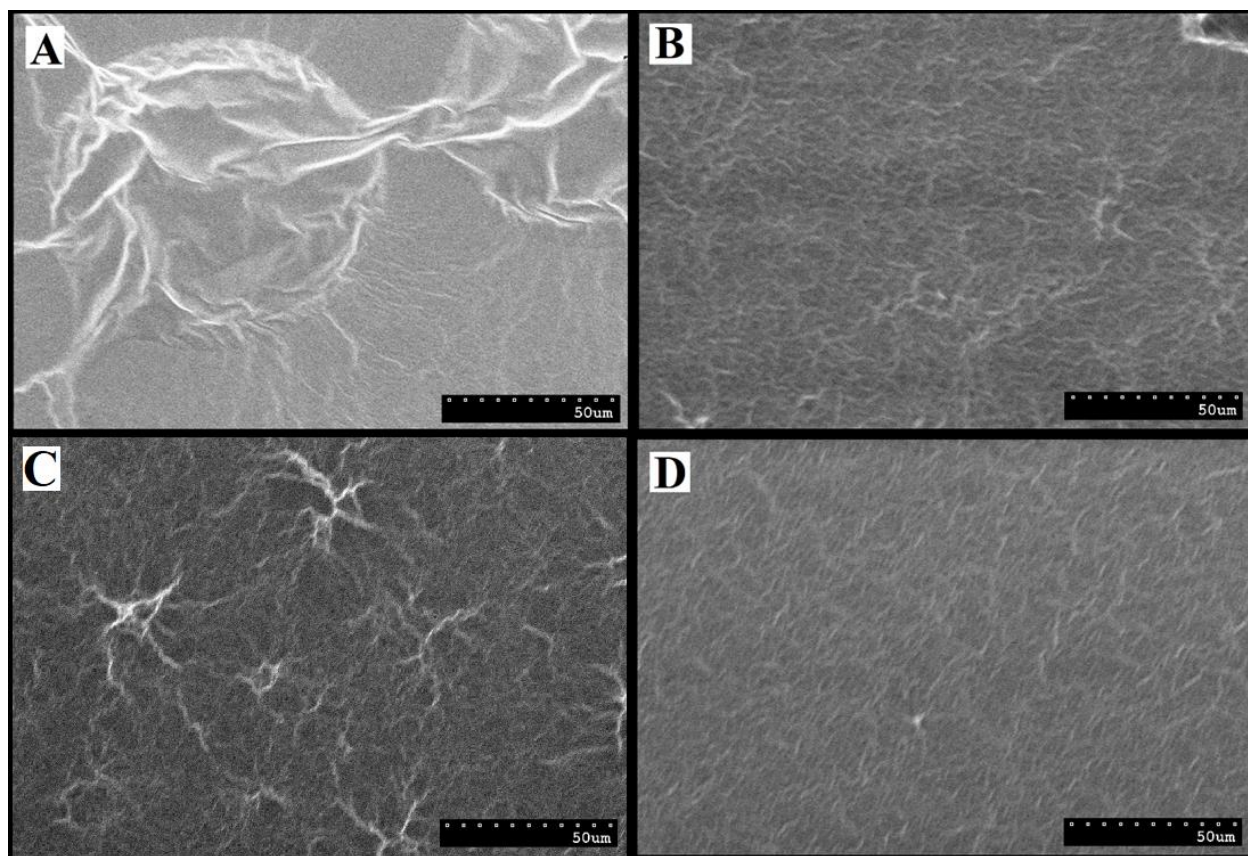


Figure 52. SEM images of films (a) DSPA_T, (b) DSPA_X, (c) ^mC DSPA_X, and (d) ^{thy}DSPA_X.

no considerable effect was detected from the UV-Vis spectra of doped DSPA_X solutions and heat-treated films. There are mild deformations that exist in throughout all DSPA_X films, possibly the consequence of the minor aggregation observed in **Figure 44**. Generally, the DSPA_X films display a semi-crystalline planar surface that is free from severe charge transfer inhibiting fragments like those observed in DSPA_T.

4.1.6 DSPA_X Film Surface Resistance

Surface resistance was determined for DSPA_X films only. Some DSPA_T films showed conductivity but were inconsistent. **Figure 53** displays bulk DSPA films. DSPA_T as mentioned previously was not homogenous, consequently films varied with most films not showing



Figure 53. Picture of DSPA bulk films.

conductivity upon heating. The films fabricated from DSPA_T exhibiting defects in through contusions, holes, and cracking, all of which had a negative impact on the conductive properties of DSPA_T. **Table 4** shows surface resistance data for DSPA_X, ^{mC}DSPA_X, and ^{thy}DSPA_X. The average $M\Omega \square^{-1}$ does not show huge differences between doped and undoped films. This is expected since doping demonstrated no significant change in UV-Vis absorbance patterns, **Figure 46**, hence the polaron transitions are relatively similar in each film. However, the secondary dopants exhibited an impact on $M\Omega \square^{-1}$ lows, with ^{mC}DSPA_X reaching $0.932 M\Omega \square^{-1}$ indicating that a few *mC* molecules may have attached to DSPA backbone. Resistivity maxima were similar for all DSPA_X films and above $5.500 M\Omega \square^{-1}$.

Table 4. Surface resistance of DSPA_x films.

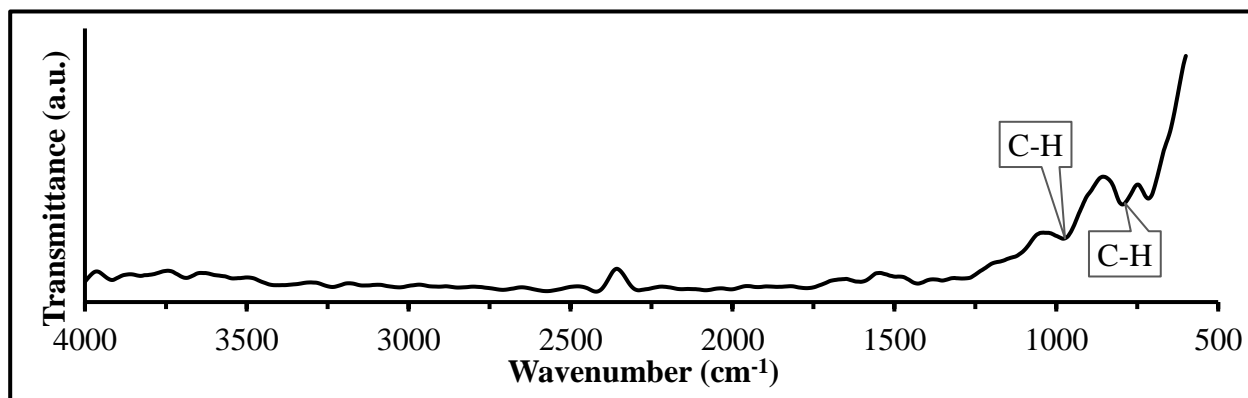
	MΩ □ ⁻¹ (avg)	MΩ □ ⁻¹ (dev)	MΩ □ ⁻¹ (low)	MΩ □ ⁻¹ (high)
DSPA _x	3.286	1.312	1.774	5.760
^m C DSPA _x	2.425	1.810	0.932	5.660
^{thy} DSPA _x	3.454	1.244	2.084	5.530

4.2 GO Materials Characterization

GO and rGO were synthesized from a variation of a modified hummers method. FTIR was used to confirm the successful synthesis of the oxide materials. GO materials are reported to form stable suspensions in water. However, in this research particle size of GO materials limit suspension stability. Therefore, the approach to stable suspension formation was investigated using optical microscopy and UV-Vis. Subsequently, the newly formed suspensions were used to make films to determine their viability as conductive materials.

4.2.1 GO Materials FTIR

Analysis of the as purchased graphite using FTIR reveals lingering impurities and aromatic deformation at 973 and 806 cm⁻¹, present in the graphite structure (**Figure 54**). An adsorption peak for CO₂ is found in all samples around 2300 cm⁻¹ which is typical for these materials exposed to

**Figure 54. FTIR of as purchased graphite.**

the atmosphere. Very broad peaks for O-H stretching of alcohols, carboxylic acids, and residual H₂O are present in the first and second synthesis of GO in the range of 3600 to 2500 cm⁻¹ (**Figures 55 and 56**). The O-H stretch is reduced in the heated treated sample of GO (Δ HGO), **Figure 57**, and removed from the rGO sample, **Figure 58**. The first GO synthesis (GO₁) has a weak C=O peak at 1728 cm⁻¹, while the second GO synthesis (GO₂) has a prominent peak at 1744 cm⁻¹, Δ HGO

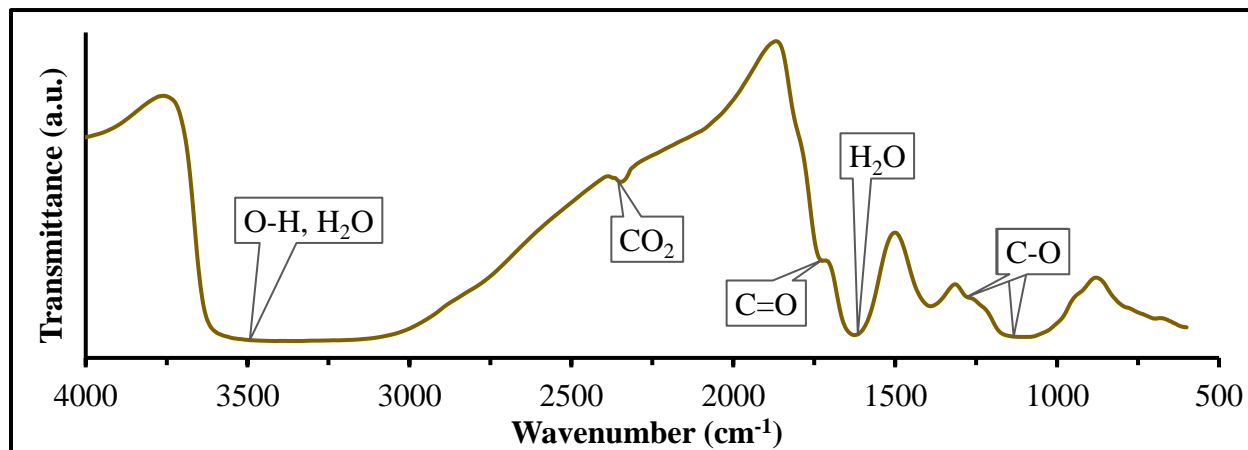


Figure 55. FTIR of GO from the first synthesis.

also shows a reduced C=O at 1744 cm⁻¹ and the peak is further reduced in rGO at 1738 cm⁻¹. Intercalated H₂O is characterized at peaks 1646, 1620, 1619, and 1597 cm⁻¹ for GO₁, GO₂, Δ HGO, and rGO respectively. The peak corresponding to C-O-C is 1278 cm⁻¹ and C-OH is 1096 cm⁻¹ for GO₁. The low intensity of C=O and C-O in GO₁ is the consequence of bulky graphite starting material (**Figure 63**) preventing the penetration and oxidation of the internal graphite consequently leading to surface oxidation only. GO₂ exhibits more intense peaks for C=O, C-O-C at 1225 cm⁻¹, and C-OH at 1078 cm⁻¹ (**Figure 56**). The increased intensity is attributed to a pre-grinding step incorporated into the modified hummers method. The heat treatment to GO₂

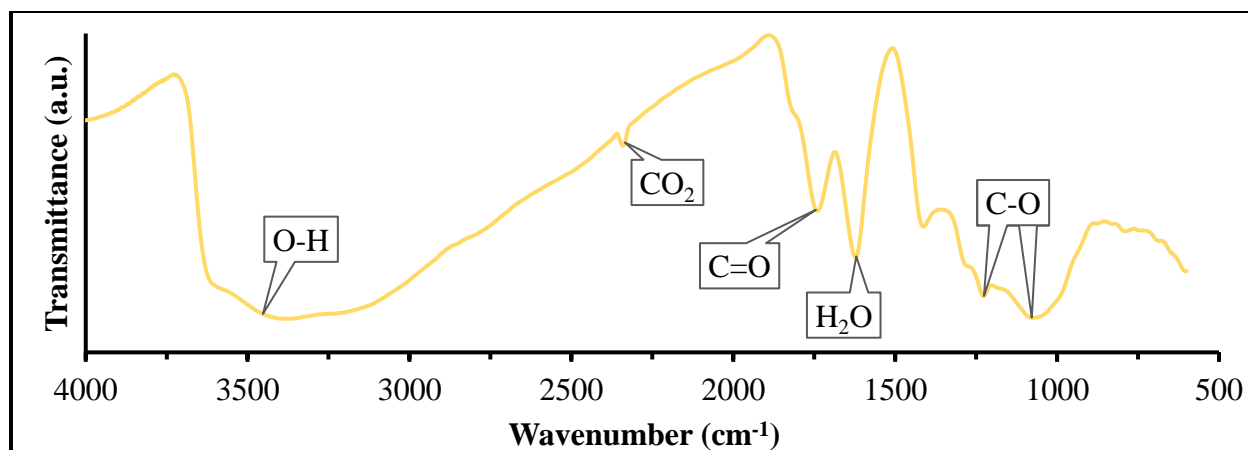


Figure 56. FTIR of GO from the second synthesis.

reduced the peak intensity of C-O-C and C-OH at 1220 and 1090 cm^{-1} respectively, for ΔHGO (Figure 57). The afore mentioned reductions of peaks for ΔHGO indicate that GO_2 has been partially reduced under vacuum at 120 $^{\circ}\text{C}$. An increase in temperature under vacuum allowed for

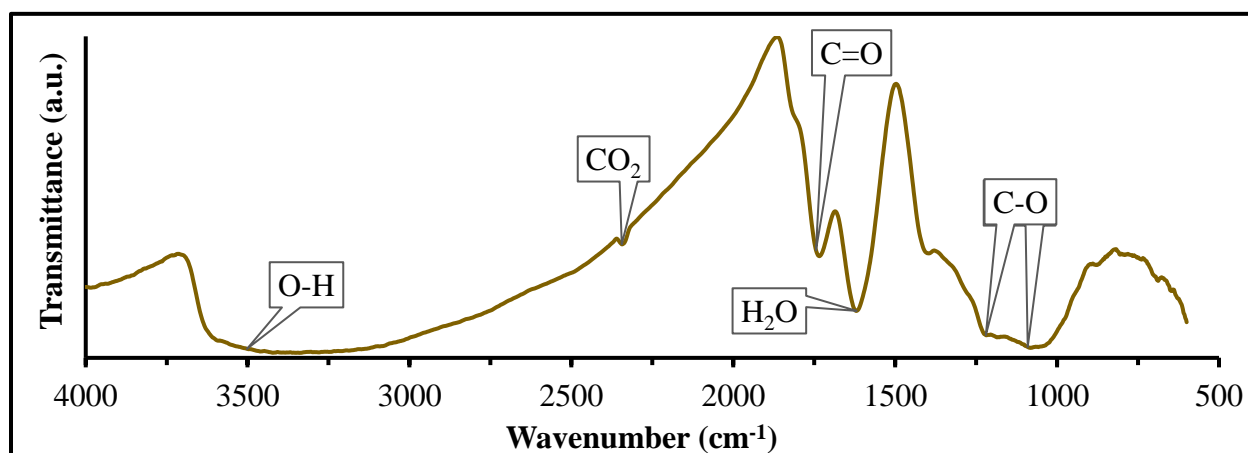


Figure 57. FTIR of heat treated GO.

an expanded reduction of GO_2 . Although the reduction process was unable to produce graphene, the resultant rGO is an excellent material with respect to the initial bulky graphite. rGO peaks corresponding to C-O-C and C-OH are at 1207 and 1053 cm^{-1} respectively (Figure 58).

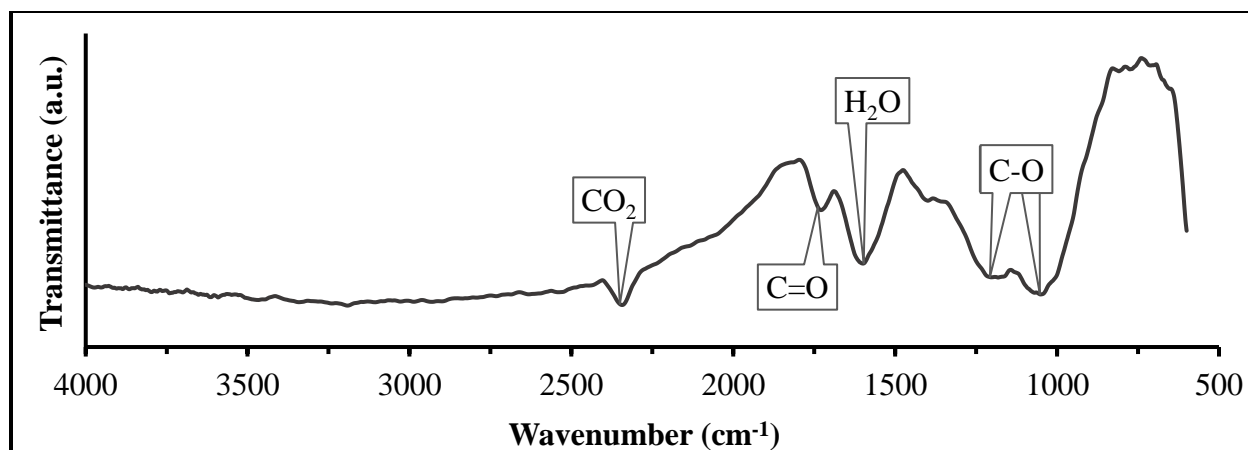


Figure 58. FTIR of thermally reduced GO.

4.2.2 GO Materials Solution UV-Vis Spectra

Suspended aqueous solutions were made using GO₁, GO₂, ΔHGO, and rGO (**Figure 59**). They were sonicated for 1 hour. Limitations in the procedure resulted in all solutions containing some particles that were unable to maintain suspension over a 24-hour period due to size. The SEM image of GO particles indicates that the size has been reduced between ungrinded, **Figure 60 (a)**, and grinded, **Figure 60 (b)**, particles. However, bulky portions remain leading to continual precipitation. Furthermore, the successful oxidation of graphite permits the formation of suspended particles. Unfortunately, GO₁ was synthesized without a pre-grinding action. Consequently, the grinding of GO₁ revealed internal portions lacking sufficient oxidation. GO₂ and its derivatives show improved suspension resulting from the enhanced oxidation of graphite. ΔHGO and rGO were used for the investigation of stable suspensions.



↓ 24 Hours ↓



Figure 59. Picture of graphite and GO materials sonicated in H₂O, taken immediately after sonication and a 24 hour period.

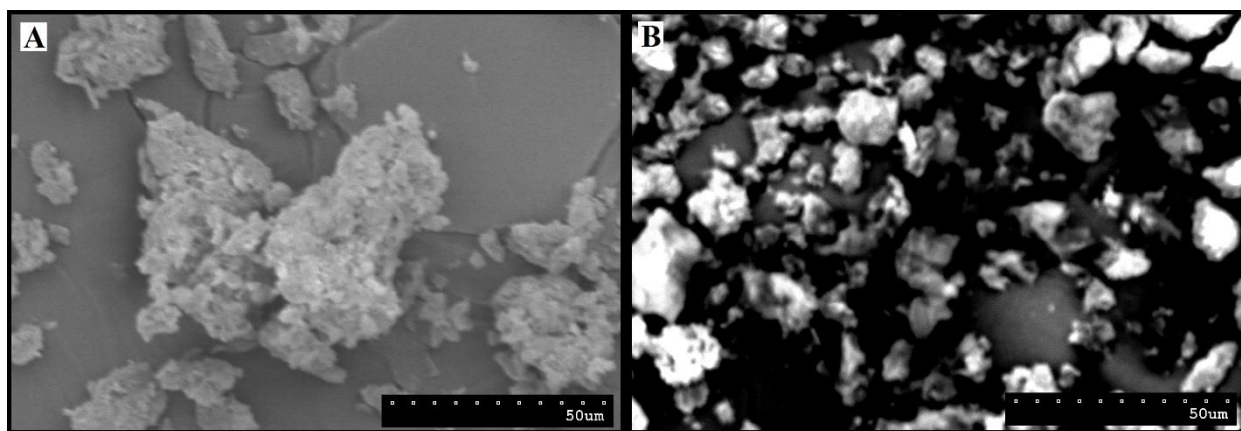


Figure 60. (a) Ungrinded GO particles and (b) grinded GO particles.

Δ HGO and rGO, after sonication, was characterized using UV-Vis on a 12-hour interval.

Figure 61 is photo image of the solutions every 12 hours detailing the progression of GO precipitation. UV-Vis spectra for both Δ HGO and rGO, **Figure 62 (a)** and **62 (b)**, expresses a

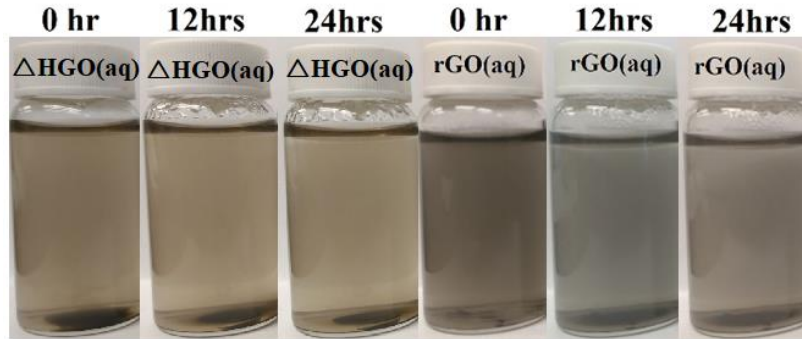


Figure 61. Δ HGO and rGO suspended solutions over 24 hours.

uniform recession of Δ HGO and rGO suspended particles, respectively. The peaks at 240 nm are representative of the ring structure found in the GO materials. The decrease in absorbance was the direct result of these particles falling out of solution. Previous literature reports the stability of GO solutions lasting over 1 month. However, those suspensions were made using nano sized GO. The GO material synthesized from commercial grade graphite has a broad range of size distribution. Some nano sized particles may exist in the commercial grade graphite but majority is bulky sized and not easily suspended.

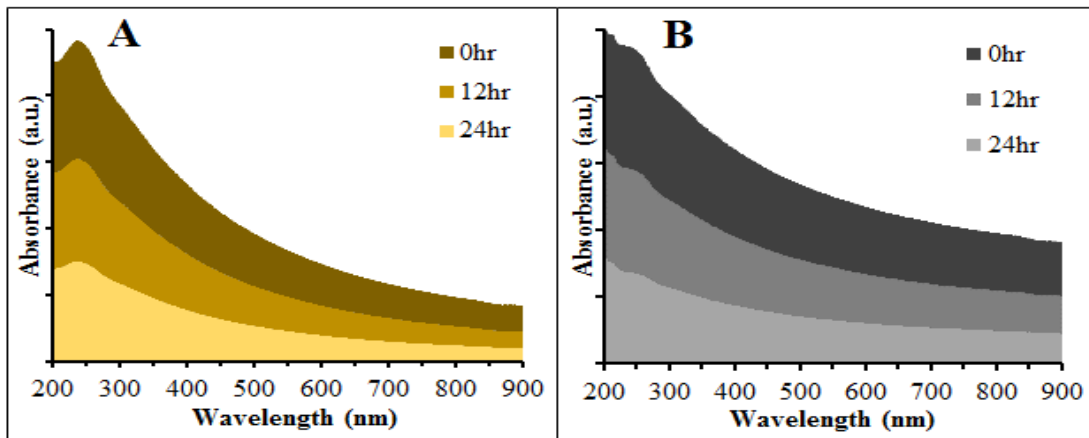


Figure 62. UV-Vis of (a) Δ HGO and (b) rGO.

4.2.3 GO Materials Optical Microscopy

Optical images of graphite, **Figure 63**, confirm that majority of the graphite material is in excess of 1 μm dimensions. Previous FTIR data, in section 4.2.1, correlates to the bulky size of graphite and the inability of penetrative oxidation. However, there are some portions of the graphite material that is nano sized. Unfortunately, this commercial grade graphite has a broad size distribution range. Thus, pre-grinding before oxidation occurs is an effective way to improve the formation of GO end products. After the successful oxidation, GO_2 and its' derivatives were able to achieve suspension in aqueous solutions.

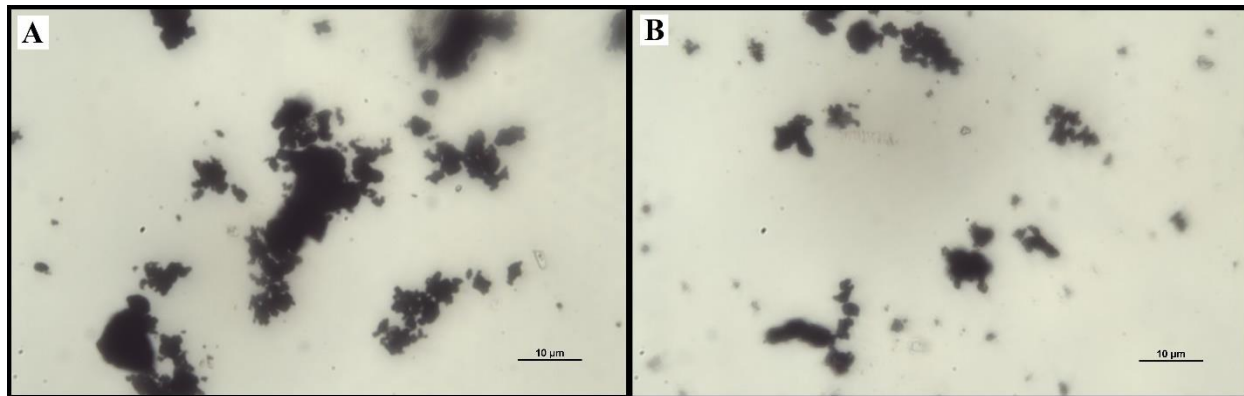


Figure 63. Optical microscopy of graphite particles.

Figure 64 highlights ΔHGO suspended over a 24-hour period. The images were taken after sonication. **Figure 64** corresponds to the aqueous solution at 0, 12, and 24 hours. They show that ΔHGO molecules are adequately well-dispersed throughout the solution. However, as time elapses the ΔHGO particles have begun their precipitation as corroborated by UV-Vis **Figure 62**. As previously stated, after grinding some particles remain above 1 micron dimensions. Accordingly, larger size molecules cannot be maintained in the suspension, but there are particles in the nano region that remain stable. At 0 hour, immediately after sonication, particles over 1 μm are visible and in large groups. 12 hours after sonication, there are visibly less particles with a noticeable

cluster. After 24 hours, particles over 1 μm are scarce but according to UV-Vis the solution still contains GO particles. The remaining portion of suspended GO is attributed to particles under 1 μm .

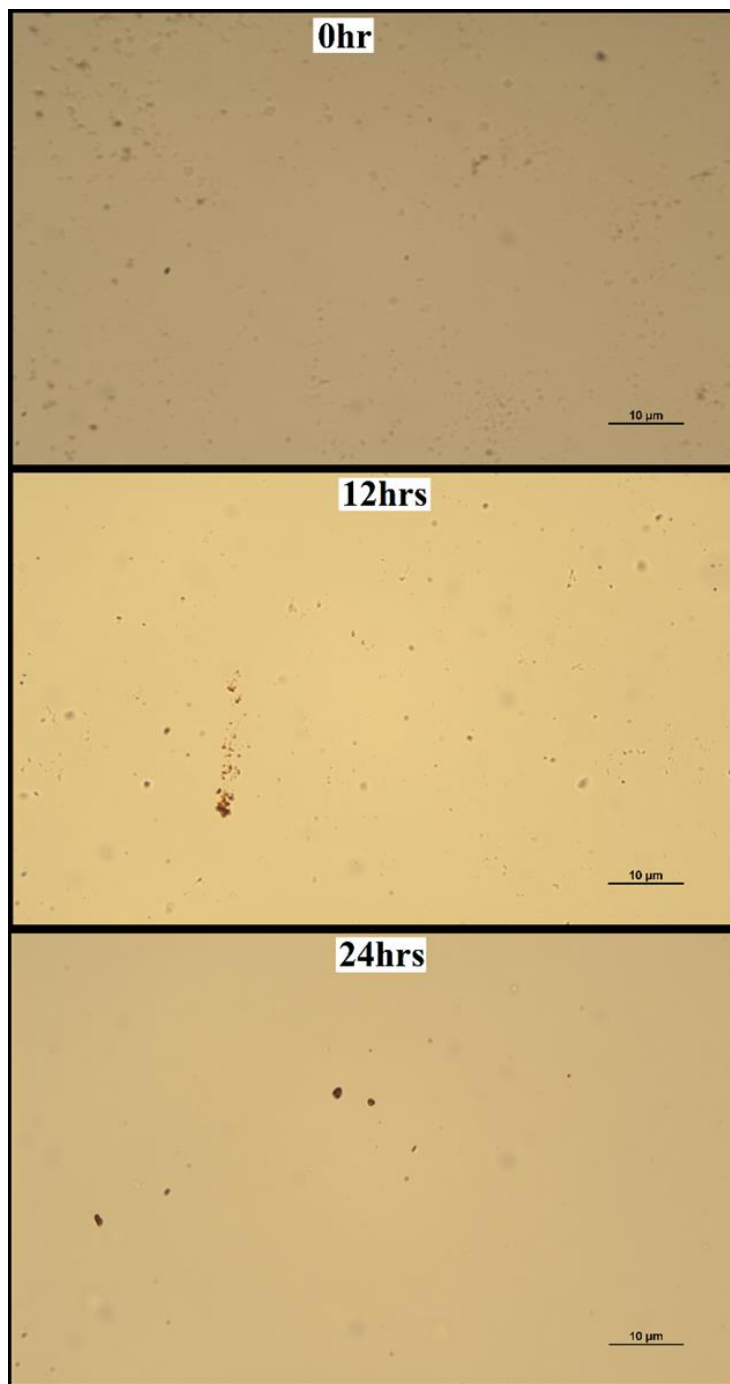


Figure 64. Optical microscopy of ΔHGO particles at 0, 12 and 24 hours.

4.2.4 GO Material Films SEM

Δ HGO films imaged with SEM display crystalline surface (**Figure 65**). The crystalline structure indicates that the molecules are packed tightly and is beneficial for the charge transfer capabilities of Δ HGO. rGO films do not exhibit the same crystalline formation as Δ HGO, instead they show a rutted amorphous surface (**Figure 66**). Cracking has been observed in portions of the rGO film (**Figure 66 (b)**). The cracking defect is the result of the removal of O-H groups through thermal treatment. The O-H groups add stability and help to increase alignment. Without the O-H rGO film is unable to maintain the uniformity expressed in Δ HGO films. The overall bulkiness of rGO and lack of O-H groups leads to the cracking phenomena. Therefore, cracking is more likely to occur at the locations with higher amounts of rGO.

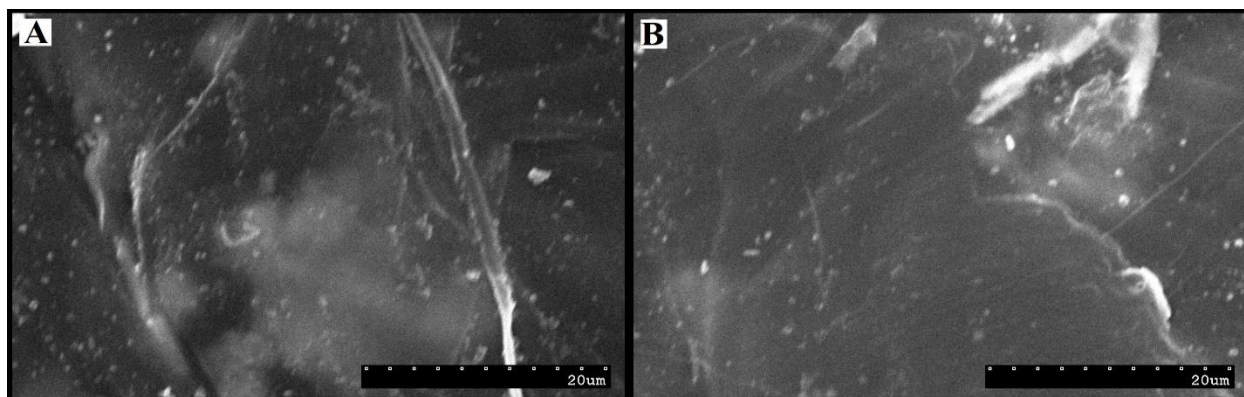


Figure 65. SEM of Δ HGO films.

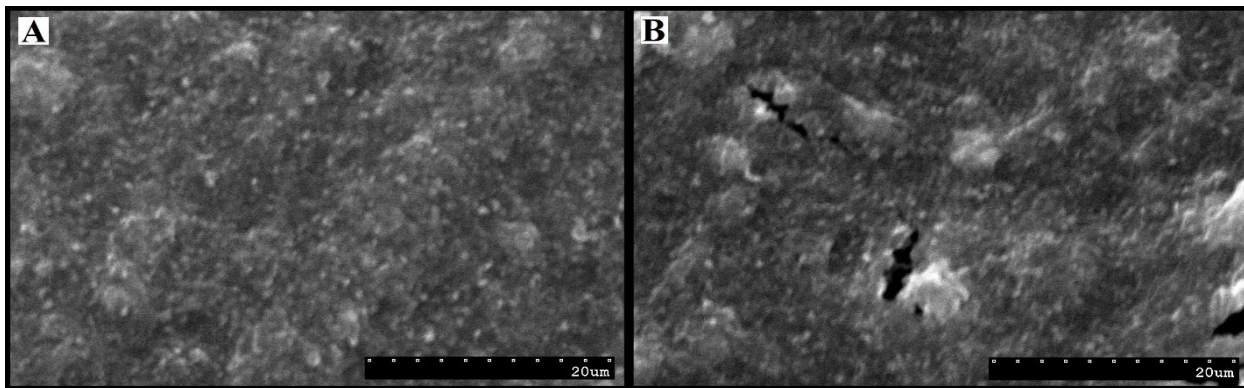


Figure 66. SEM of rGO films.

4.2.5 GO Materials Surface Resistance

Δ HGO and rGO films exhibited complete differences in surface resistance measurements, with the former showing conductivity, **Table 5**, and the latter unable to maintain stability. The difference can be attributed to the contrasting films. Δ HGO film is crystalline and highly packed while rGO film is amorphous and susceptible to cracking. Δ HGO averaged $3.902 \text{ M}\Omega \square^{-1}$ dropping to a low of $3.144 \text{ M}\Omega \square^{-1}$ and showing superior capabilities over rGO films. However, rGO should be the better charge transfer carrier but due to the bulkiness of the developed films high performances were not achieved.

Table 5. Surface resistance of GO materials.

	$\text{M}\Omega \square^{-1}$ (avg)	$\text{M}\Omega \square^{-1}$ (dev)	$\text{M}\Omega \square^{-1}$ (low)	$\text{M}\Omega \square^{-1}$ (high)
Δ HGO	3.902	0.458	3.144	4.446

CHAPTER 5. CONCLUSION

5.1 Summary

PANI and GO materials were successfully synthesized from newly incorporated fabrication steps. DSS improved the solubility of PANI as expected from the long alkyl molecule. However, DSS severely inhibited the attempts at secondary doping through over saturation on the polymer backbone or steric hindrance from the alkyl branch. DSPA in toluene solvent showed a decrease in dispersion, correspondingly increasing in aggregation with micelle formation. Ortho-xylene showed positive impact by preventing the major defects occurring in DSPA_T.

The GO synthesis was augmented to include alternative materials for production. Semi-stable GO suspensions were formed in aqueous solutions. The bulky graphite starting material was found to have a significant effect on the formation of stable suspension. This limitation was partially alleviated through the manual grinding of graphite prior to synthesis. Subsequently, GO was successfully reduced using thermal treatment under vacuum forming Δ HGO and rGO. Δ HGO films displayed a crystalline surface and improved conductive properties over rGO films due to the presence of O-H groups and hydrogen bonding availability. The lack of O-H groups in rGO prevented the alignment particles consequently leading to fractures in the film. There is potential in using commercial grade graphite for the synthesis of GO. The methods and applications need to be developed accordingly.

REFERENCES

- [1] Krupp, F.; Horn, M. *Earth: The Sequel*; W.W. Norton and Company: New York, 2008.
- [2] Janardhan, V.; Fesmire, B. *Energy Explained Volume 1 Conventional Energy*; Rowman and Littlefield: Lanham, 2011.
- [3] The Shift Project. Breakdown of Energy Production Statistics. <http://www.tsp-data-portal.org/Breakdown-of-Energy-Production-Statistics#tspQvChart> (accessed Feb 11, 2017).
- [4] Goldemberg, J. *Energy What Everyone Needs to Know*; Oxford University Press: New York, 2012.
- [5] The Shift Project. Breakdown of CO2 Emissions from Energy Consumption. <http://www.tsp-data-portal.org/Breakdown-of-CO2-Emissions-from-energy-consumption#tspQvChart> (accessed Feb 11, 2017).
- [6] U.S. Energy Information Administration. International Energy Outlook 2016. [https://www.eia.gov/outlooks/ieo/pdf/0484\(2016\).pdf](https://www.eia.gov/outlooks/ieo/pdf/0484(2016).pdf) (accessed Feb 23, 2017).
- [7] Carraher Jr., C. E. *Introduction to Polymer Chemistry*; CRC Press Taylor and Francis Group: Boca Raton, 2007.
- [8] Stevens, M. P. *Polymer Chemistry An Introduction*, 3rd ed.; Oxford University Press: New York, 1999.
- [9] Bubnova, O.; Khan, Z. U.; Wang, H.; Braun, S.; Evans, D. R.; Fabretto, M.; Hojati-Talemi, P.; Dagnelund, D.; Arlin, J. B.; Geerts, Y. H.; Desbief, S.; Breiby, D. W.; Andreasen, J. W.; Lazzaroni, R.; Chen, W. M.; Zozoulenko, I.; Fahlman, M.; Murphy, P. J.; Berggren, M.; Crispin, X. Semi-Metallic Polymers. *Nature Materials*. **2013**, *13*, 190-194.
- [10] Walton, D.J. Electrically Conducting Polymers. *Materials and Design*. **1990**, *11*, 142-152.

- [11] Kumar, D.; Sharma, R. C. Advances in Conductive Polymers. *European Polymer Journal*, **1998**, *34*, 1053-1060.
- [12] MacDiarmid, A. G. Synthetic Metals: A Novel Role for Organic Polymers. *Synthetic Metals*. **2001**, *125*, 11-22.
- [13] Sengodu, P.; Deshmukh, A. Conducting Polymers and Their Inorganic Composites for Advanced Li-Ion Batteries: A Review. *The Royal Society of Chemistry Advances*. **2015**, *5*, 42109-42130.
- [14] Muehllbacher, D.; Koppe, M.; Denk, P.; Waldauf, C.; Heeger, A. J.; Brabec, C. J.; Scharber, M. C. Design Rules for Donors in Bulk-Heterojunction Solar Cells-Towards 10% Energy-Conversion Efficiency. *Advanced Materials*. **2006**, *18*, 789-794.
- [15] You, J.; Dou, L.; Yoshimura, K.; Kato, T.; Ohya, K.; Moriarty, T.; Emery, K.; Chen, C. C.; Gao, J.; Li, G.; Yang, Y. A Polymer Tandem Solar Cell With 10.6% Power Conversion Efficiency. *Nature Communications*. **2013**, *4*, 1446-1454.
- [16] Krebs, F. C. Fabrication and Processing of Polymer Solar Cells: A Review of Printing and Coating Techniques. *Solar Energy Materials and Solar Cells*. **2009**, *93*, 394-412.
- [17] Chen, H. Y.; Hou, J.; Zhang, S.; Liang, Y.; Yang, G.; Yang, Y.; Yu, L.; Wu, Y.; Li, G. Polymer Solar Cells with Enhanced Open-Circuit Voltage and Efficiency. *Nature Photonics*. **2009**, *3*, 649-653.
- [18] Sondergaard, R.; Hosel, M.; Angmo, D.; Larsen-Olsen, T.T.; Krebs, F.C. Roll-to-Roll Fabrication of Polymer Solar Cells. *Materials Today*. **2012**, *15*, 36-49.
- [19] Riede, M.; Uhrich, C.; Widmer, J.; Timmreck, R.; Wynands, D.; Schwartz, G.; Gnehr, W. M.; Hildebrandt, D.; Weiss, A.; Hwang, J.; Sundarraj, S.; Erk, P.; Pfeiffer, M.; Leo, K. Efficient

- Organic Tandem Solar Cells based on Small Molecules. *Advanced Functional Materials*. **2011**, *21*, 3019-3028.
- [20] Chen, C. C.; Chang, W. H.; Yoshimura, K.; Ohya, K.; You, J.; Gao, J.; Hong, Z.; Yang, Y. An Efficient Triple-Junction Polymer Solar Cell Having a Power Conversion Efficiency Exceeding 11%. *Advanced Materials*. **2014**, *26*, 5670-5677.
- [21] Kawashima, K.; Tamai, Y.; Ohkita, H.; Osaka, I.; Takimiya, K. High-Efficiency Polymer Solar Cells with Small Photon Energy Loss. *Nature Communications*. **2015**, *6*, 10085-10092.
- [22] U.S. Department of Energy. Types of Fuel Cells. <https://energy.gov/eere/fuelcells/types-fuel-cells> (accessed Apr 12, 2017).
- [23] Kraysberg, A.; Ein-Eli, Y. Review of Advanced Materials for Proton Exchange Membrane Fuel Cells. *Energy and Fuels*. **2014**, *28*, 7303-7330.
- [24] Miyatake, K.; Chikashige, Y.; Higuchi, E.; Watanabe, M. Tuned Polymer Electrolyte Membranes Based on Aromatic Polyethers for Fuel Cell Applications. *Journal of the American Chemical Society*. **2007**, *129*, 3879-3887.
- [25] Si, K.; Wycisk, R.; Dong, D.; Cooper, K.; Rodgers, M.; Brooker, P.; Slattery, D.; Litt, M. Rigid-Rod Poly(phenylenesulfonic acid) Proton Exchange Membranes with Cross-Linkable Biphenyl Groups for Fuel Cell Applications. *Macromolecules*. **2013**, *46*, 422-433.
- [26] Mader, J. A.; Benicewicz, B. C. Sulfonated Polybenzimidazoles for High Temperature PEM Fuel Cells. *Macromolecules*. **2010**, *43*, 6706-6715.
- [27] Novak, P.; Muller, K.; Santhanam, K. S. V.; Haas, O. Electrochemically Active Polymers for Rechargeable Batteries. *Chemical Reviews*. **1997**, *97*, 207-281.
- [28] Muench, S.; Wild, A.; Friebe, C.; Häupler, B.; Janoschka, T.; and Schubert, U. S. Polymer-Based Organic Batteries. *Chemical Reviews*. **2016**, *116*, 9438-9484.

- [29] Forse, A. C.; Merlet, C.; Griffin, J. M.; Grey, C. P. New Perspectives on the Charging Mechanisms of Supercapacitors. *Journal of the American Chemical Society*. **2016**, *318*, 5731-5744.
- [30] Liu, C.; Yu, Z.; Neff, D.; Zhamu, A.; Jang, B. Z. Graphene-Based Supercapacitor with an Ultrahigh Energy Density. *Nano Letters*. **2010**, *10*, 4863-4868.
- [31] Anothumakkool, B.; Torris A. T., A.; Veeliyath, S.; Vijayakumar, V.; Badiger, M.V.; Kurungot, S. High-Performance Flexible Solid-State Supercapacitor with an Extended Nanoregime Interface through in Situ Polymer Electrolyte Generation. *ACS Applied Materials and Interfaces*. **2016**, *8*, 1233-1241.
- [32] Zeigler, D. F.; Candelaria, S. L.; Mazzio, K. A.; Martin, T. R.; Uchaker, E.; Suraru, S. L.; Kang, L. J.; Cao, G.; Luscombe, C. K. N-Type Hyperbranched Polymers for Supercapacitor Cathodes with Variable Porosity and Excellent Electrochemical Stability. *Macromolecules*. **2015**, *48*, 5196-5203.
- [33] Xia, X.; Chao, D.; Fan, Z.; Guan, C.; Cao, X.; Zhang, H.; Fan, H. J. A New Type of Porous Graphite Foams and Their Integrated Composites with Oxide/Polymer Core/Shell Nanowires for Supercapacitors: Structural Design, Fabrication, and Full Supercapacitor Demonstrations. *Nano Letters*. **2014**, *14*, 1651-1658.
- [34] Yin, Y.; Feng, K.; Liu, C.; Fan, S. A Polymer Supercapacitor Capable of Self-Charging under Light Illumination. *The Journal of Physical Chemistry C*. **2015**, *119*, 8488-8491.
- [35] MacDiarmid, A. G. Nobel Lecture: "Synthetic Metals": A Novel Role for Organic Polymers. *Angewandte Chemie International Edition*. **2001**, *125*, 2581-2590.

- [36] Chiang, C. K.; Fincher Jr., C. R.; Park, Y. W.; Heeger, A. J.; Shirakawa, H.; Louis, E. J.; Gau, S. C.; MacDiarmid, A. G. Electrical Conductivity in Doped Polyacetylene. *Physical Review Letters*. **1977**, *39*, 1098-1101.
- [37] Chiang, C. K.; Park, Y. W.; Heeger, A. J.; Shirakawa, H.; Louis, E. J.; MacDiarmid, A. G. Conducting Polymers: Halogen Doped Polyacetylene. *The Journal of Chemical Physics*. **1978**, *69*, 5098-5104.
- [38] Nigrey, P. J.; MacInnes, D.; Nairns, D. P.; Heeger, A. J.; MacDiarmid, A. G. Lightweight Rechargeable Storage Batteries Using Polyacetylene, (CH) x as the Cathode-Active Material. *Journal of the Electrochemical Society*. **1981**, *128*, 1651-1654.
- [39] Heeger, A. J.; Nigrey, P. J.; MacDiarmid, A. G. Batteries Having Conjugated Polymer Electrodes. US 4442187 A, April 10, 1984.
- [40] MacDiarmid, A. G.; Chiang, J. C.; Halpern, M.; Huang, W. S.; Mu, S. L.; Nanaxakkara, L. D.; Wu, S. W.; Yaniger, S. I. "Polyaniline": Interconversion of Metallic and Insulating Forms. *Molecular Crystals and Liquid Crystals*. **1985**, *121*, 173-180.
- [41] MacDiarmid, A. G.; Mu, S. L.; Nanaxakkara, L. D.; Wu, W. Electrochemical Characteristics of "Polyaniline" Cathodes and Anodes in Aqueous Electrolytes. *Molecular Crystals and Liquid Crystals*. **1985**, *121*, 187-190.
- [42] MacDiarmid, A. G.; Chiang, J. C.; Richard, A. F.; Somasiri, N. L. D. Synthesis and Characterization of Emeraldine Oxidation State by Elemental Analysis. *Conducting Polymers*. 1987, 105-120.
- [43] MacDiarmid, A. G.; Chiang, J. C.; Richter, A. F.; Epstein, A. J. Polyaniline: A New Concept in Conducting Polymers. *Synthetic Metals*. 1987, *18*, 285-290.
- [44] MacDiarmid, A. G. High Capacity Polyaniline Electrodes. US 4940640 A, July 10, 1990.

- [45] Asturias, G. E.; Jang, G. W.; Macdiarmid, A. G.; Doblhofer, K.; Zhong, C. Membrane-Properties of Polymer Films: The Acid-Doping Reaction of Polyaniline. *Bunsengesellschaft für Physikalische Chemie*. **1991**, 95,1381-1384.
- [46] MacDiarmid, A. G.; Epstein, A. J. Conducting Polymers: Past, Present and Future... *MRS Proceedings*. **1993**, 328, 133.
- [47] Wei, Y.; Tian, J.; MacDiarmid, A. G.; Masters, J. G.; Smith, A. L.; Li, D. Preparation and Conductivities of Fullerene-Doped Polyanilines. *Journal of the Chemical Society, Chemical Communications*. **1993**, 603-604.
- [48] MacDiarmid, A. G.; Epstein, A. J. The Concept of Secondary Doping as Applied to Polyaniline. *Synthetic Metals*. **1994**, 65, 103-116.
- [49] MacDiarmid, A. G.; Xia, Y. N.; Wiesinger, J. M. Methods for Preparing Conductive Polyanilines. US 5403913 A, April 4, 1995.
- [50] Huang, Z.; Wang, P. C.; MacDiarmid, A. G.; Xia, Y.; Whitesides, G. Selective Deposition of Conducting Polymers on Hydroxyl-Terminated Surfaces with Printed Monolayers of Alkylsiloxanes as Templates. *Langmuir*. **1997**, 13, 6480-6484.
- [51] Kane-Maguire, L. A. P.; MacDiarmid, A. G.; Norris, I. D.; Wallace, G. G.; Zheng, W. Facile Preparation of Optically Active Polyanilines via the In Situ Chemical Oxidative Polymerisation of Aniline. *Synthetic Metals*. **1999**, 106, 171-176.
- [52] Shimano, J. Y.; MacDiarmid, A. G. Polyaniline, a Dynamic Block Copolymer: Key to Attaining its Intrinsic Conductivity? *Synthetic Metals*. **2001**, 123, 251-262.
- [53] Hohnholz, D.; Okuzaki, H.; MacDiarmid, A. G. Plastic Electronic Devices through Line Patterning of Conducting Polymers. *Advanced Functional Materials*. **2005**, 15, 51-56.

- [54] Wang, P. C.; Venancio, E. C.; Sarno, D. M.; MacDiarmid, A. G. Simplifying the Reaction System for the Preparation of Polyaniline Nanofibers: Re-examination of Template-Free Oxidative Chemical Polymerization of Aniline in Conventional Low-pH Acidic Aqueous Media. *Reactive and Functional Polymers*. **2009**, *69*, 217-223.
- [55] Inzelt, G. *Conducting Polymers: A New Era in Electrochemistry*, 2nd ed.; Springer: New York, 2012.
- [56] Parker, P. M. *Polyaniline: Webster's Timeline History, 1974-2007*; UCON Group International: San Diego, 2009.
- [57] Zhao, H. B.; Yuan, L.; Fu, Z. B.; Wang, C. Y.; Yang, X.; Zhu, J. Y.; Qu, J.; Chen, H. B.; Schiraldi, D. A. Biomass-Based Mechanically Strong and Electrically Conductive Polymer Aerogels and Their Application for Supercapacitors. *ACS Applied Materials and Interfaces*. **2016**, *8*, 9917-9924.
- [58] Chen, D.; Miao, Y. E.; Liu, T. Electrically Conductive Polyaniline/Polyimide Nanofiber Membranes Prepared via a Combination of Electrospinning and Subsequent In Situ Polymerization Growth. *ACS Applied Materials and Interfaces*. **2013**, *5*, 1206-1212.
- [59] Xie, J.; Han, X.; Ji, H.; Wang, J.; Zhao, J.; Lu, C. Self-Supported Crack-Free Conducting Polymer Films with Stabilized Wrinkling Patterns and Their Applications. *Scientific Reports*. **2016**, *6*, 1038-1049.
- [60] Yue, Y.; Yang, Z.; Liu, N.; Liu, W.; Zhang, H.; Ma, Y.; Yang, C.; Su, J.; Li, L.; Long, F.; Zou, Z.; Gao, Y. A Flexible Integrated System Containing a Microsupercapacitor, a Photodetector, and a Wireless Charging Coil. *ACS Nano*. **2016**, *10*, 11249-11257.

- [61] Abdelhamid, M. E.; Snokk, G. A.; O'Mullane, A. P. Electrochemical Tailoring of Fibrous Polyaniline and Electroless Decoration with Gold and Platinum Nanoparticles. *Langmuir*. **2016**, 32, 8834-8842.
- [62] Simotwo, S. K.; DelRe, C.; Kalra, V. Supercapacitor Electrodes Based on High-Purity Electrospun Polyaniline and Polyaniline-Carbon Nanotube Nanofibers. *ACS Applied Materials and Interfaces*. **2016**, 8, 21261-21269.
- [63] Du, P.; Liu, H. C.; Yi, C.; Wang, K.; Gong, X. Polyaniline-Modified Oriented Graphene Hydrogel Film as the Free-Standing Electrode for Flexible Solid-State Supercapacitors. *ACS Materials and Interfaces*. **2015**, 7, 23932-23940.
- [64] Cong, H. P.; Ren, X. C.; Wang, P.; Yu, S. H. Flexible Graphene-Polyaniline Composite Paper for High-Performance Supercapacitor. *Energy and Environmental Science*. **2013**, 6, 1185-1191.
- [65] Grover, S.; Goel, S.; Sahu, V.; Singh, G.; Sharma, R. K. Asymmetric Supercapacitive Characteristics of PANI Embedded Holey Graphene Nanoribbons. *ACS Sustainable Chemistry and Engineering*. **2015**, 3, 1460-1469.
- [66] Wang, L.; Feng, X.; Ren, L.; Piao, Q.; Zhong, J.; Wang, Y.; Li, H.; Chen, Y.; Wang, B. Flexible Solid-State Supercapacitor Based on a Metal–Organic Framework Interwoven by Electrochemically-Deposited PANI. *Journal of the American Chemical Society*. **2015**, 137, 4920-2923.
- [67] Feng, M.; Tian, J.; Xie, H.; Kang, Y.; Shan, Z. Nano-Silicon/Polyaniline Composites with an Enhanced Reversible Capacity as Anode Materials for Lithium Ion Batteries. *Journal of Solid State Electrochemistry*. **2015**, 19, 1773-1782.

- [68] Aubrey, M. L.; Long, J. R. A Dual-Ion Battery Cathode via Oxidative Insertion of Anions in a Metal-Organic Framework. *Journal of the American Chemical Society*. **2015**, *137*, 13594-13602.
- [69] Molapo, K. M.; Ndangli, P. M.; Ajayi, R. F.; Mbambisa, G.; Mailu, S. M.; Njomo, N.; Masikini, M.; Baker, P.; Iwuoha, E. I. Electronics of Conjugated Polymers (I): Polyaniline. *International Journal of Electrochemical Science*. **2012**, *7*, 11859-11875.
- [70] Bhadra, S. Polyaniline: Preparation, Properties, Processing and Applications; LAP LAMBERT Academic Publishing: Saarbrucken, 2010.
- [71] Ramesha, G. K.; Kumara, A. V.; Sampath, S. In Situ Electrochemical Polymerization at Air-Water Interface: Surface-Pressure-Induced, Graphene-Oxide-Assisted Preferential Orientation of Polyaniline. *The Journal of Physical Chemistry C*. **2012**, *116*, 13997-14004.
- [72] Pina, C. D.; Falletta, E. Polyaniline From Tradition to Innovation; Nova Science Publishers: New York, 2015.
- [73] Karyakin, A. A.; Maltsev, I. A.; Lukachova, L. V. The Influence of Defects in Polyaniline Structure on its Electroactivity: Optimization of 'Self-Doped' Polyaniline Synthesis. *Journal of Electroanalytical Chemistry*. **1996**, *402*, 217--219.
- [74] Chiang, J. C.; MacDiarmid, A. G. Polyaniline: Protonic Acid Doping of the Emeraldine Form to the Metallic Regime. *Synthetic Metals*. **1986**, *13*, 193-205.
- [75] Chiang, J. C.; Huang, W.; Humphrey, B. D.; Somasiri, N. L. D. MacDiarmid, A. G. Polyaniline: Protonic Acid Doping to the Metallic Regime. *Molecular Crystals and Liquid Crystals*. **1985**, *125*, 309-318.
- [76] Matveeva, E. S. Could the Acid Doping of Polyaniline Represent the Charge Transfer Interaction. *Synthetic Metals*. **1996**, *83*, 89-96.

- [77] MacDiarmid, A. G. Secondary Doping: A New Concept in Conducting Polymers. *Macromolecular Symposia*. **1995**, 98, 835-842.
- [78] Macdiarmid, A. G.; Chiang, J. C.; Richter, A. F.; Epstein, A. J. Polyaniline: A New Concept in Conducting Polymers. *Synthetic Metals*. **1987**, 18, 285-290.
- [79] Liu, J.; Ding, Y.; Graham, C. R.; Remsen, E. E.; Kinlen P. J. Emulsion Polymerization Process for Organically Soluble and Electrically Conducting Polyaniline. *Macromolecules*. **1998**, 31, 1735-1744.
- [80] Frushour, B. G.; Ding, Y.; Menon, V.; Kinlen P. J. Synthesis and Characterization of Organically Soluble Polyaniline and Polyaniline Block Copolymers. *Synthetic Metals*. **1999**, 10, 758-761.
- [81] Lee, K. S.; Hino, T.; Kuramoto, N. Highly Conductive Polyaniline Doped with DEHSSA Synthesized in Different Protonic Acids. *Chemistry Letters*. **2007**, 36, 340-341.
- [82] Fu, Y.; Elsenbaumer, R. L. Thermochemistry and Kinetics of Chemical Polymerization of Aniline Determined by Solution Calorimetry. *Chemistry of Materials*. **1994**, 6, 671-677.
- [83] Mateeva, E.; Parkhutik, V. P. Effects of Molecular Doping by Hydroquinones on Morphology and Optical Properties of Polyaniline. *The Journal of Physical Chemistry B*. **1998**, 102, 1549-1555.
- [84] Wakeman, R. J.; Hellgardt, K.; Gupta, Y. Enhanced Permeability of Polyaniline Based Nano-Membranes for Gas Separation. *Journal of Membrane Science*. **2006**, 282, 60-70.
- [85] Dreyer, D. R.; Park, S.; Bielawski, C. W.; Ruoff, R. S. The Chemistry of Graphene Oxide. *Chemical Society Reviews*. **2010**, 39, 228-240.

- [86] Dimiev, A. M.; Eigler, S. Graphene Oxide Fundamentals and Applications. In *Graphite Oxide Story – From the Beginning Till the Graphene Hype*; Lerf, A.; Wiley: West Sussex, 2017; p 3-6.
- [87] Zhu, Y.; Murali, S.; Cai, W.; Li, X.; Suk, J. W.; Potts, J. R.; Ruoff, R. S. Graphene and Graphene Oxide: Synthesis, Properties, and Applications. *Advanced Materials*. **2010**, *22*, 3906-3924.
- [88] Shao, G.; Lu, Y.; Wu, F.; Yang, C.; Zeng, F.; Wu, Q. Graphene Oxide: The Mechanisms of Oxidation and Exfoliation. *Journal of Materials Science*. **2012**, *47*, 4400-4409.
- [89] Park, S.; Mohanty, N.; Suk, J. W.; Nagaraja, A.; An, J.; Piner, R. D.; Cai, W.; Dreyer, D. R.; Berry, V.; Ruoff, R. S. Biocompatible, Robust Free-Standing Paper Composed of a TWEEN/Graphene Composite. *Advanced Materials*. **2010**, *22*, 1736-1740.
- [90] Hu, N.; Wang, Y.; Chai, J.; Gao, R.; Yang, Z.; Kong, E. S. W.; Zhang, Y. Gas Sensor Based on p-Phenylenediamine Reduced Graphene Oxide. *Sensors and Actuators B: Chemical*. **2012**, *163*, 107-114.
- [91] Loh, K. P.; Tong, S. W.; Wu, J. Graphene and Graphene-like Molecules: Prospects in Solar Cells. *Journal of the American Chemical Society*. **2016**, *138*, 1095-1102.
- [92] Marcano, D. C.; Kosynkin, D. V.; Berlin, J. M.; Sinitskii, A.; Sun, Z.; Slesarev, A.; Alemany, L. B.; Lu, W.; Tour, J. M. Improved Synthesis of Graphene Oxide. *ACS Nano*. **2010**, *4*, 4806-4814.
- [93] Sumboja, A.; Foo, C. Y.; Wang, X.; Lee, P. S.; Large Areal Mass, Flexible and Free-Standing Reduced Graphene Oxide/Manganese Dioxide Paper for Asymmetric Supercapacitor Device. *Advanced Materials*. **2013**, *25*, 2809-2815.

- [94] Eda, G.; Fanchini, G.; Chhowalla, M. Large-area Ultrathin Films of Reduced Graphene Oxide as a Transparent and Flexible Electronic Material. *Nature Nanotechnology*. **2008**, *3*, 270-274.
- [95] Kovtyukhova, N. I.; Ollivier, P. J.; Martin, B. R.; Mallouk, T. E.; Chizhik, S. A.; Buzaneva, E. V.; Gorchinskiy, A. D. Layer-by-Layer Assembly of Ultrathin Composite Films from Micron-Sized Graphite Oxide Sheets and Polycations. *Chemistry of Materials*. **1999**, *11*, 771-778.
- [96] Dimiev, A. M.; Eigler, S. Graphene Oxide Fundamentals and Applications. In *Characterization Techniques*; Dimiev, A. M.; Eigler, S.; Wiley: West Sussex, 2017; p 95.
- [97] Tang, L.; Li, X.; Du, D.; He, C. Fabrication of Multilayer Films from Regenerated Cellulose and Graphene Oxide Through Layer-by-Layer Assembly. *Progress in Natural Science: Materials International*. **2012**, *22*, 341-346.
- [98] Xu, J.; Wang, K.; Z, S. Z.; Han, B. H.; Wei, Z. Hierarchical Nanocomposites of Polyaniline Nanowire Arrays on Graphene Oxide Sheets with Synergistic Effect for Energy Storage. *ACS Nano*. **2010**, *4*, 5019-5026.

